

**CZECH TECHNICAL UNIVERSITY IN
PRAGUE**

Faculty of Civil Engineering



**DETERMINATION OF METHOD FOR
INVESTIGATION OF IRRADIATION-
INDUCED STEEL-CONCRETE INTERFACE
DEGRADATION**

Diploma thesis

2018/2019

Bc. Denisa Kavanová



ČESKÉ VYSOKÉ UČENÍ TECHNICKÉ V PRAZE



Fakulta stavební
Thákurova 7, 166 29 Praha 6

ZADÁNÍ DIPLOMOVÉ PRÁCE


I. OSOBNÍ A STUDIJNÍ ÚDAJE

Příjmení: Kavanová	Jméno: Denisa	Osobní číslo: 421391
Zadávatel: katedra: K133		
Studijní program: Stavební inženýrství		
Studijní obor: Konstrukce pozemních staveb		

II. ÚDAJE K DIPLOMOVÉ PRÁCI

Název diplomové práce: Stanovení metody pro zkoumání degradace rozhraní oceli a betonu způsobené ozářením	
Název diplomové práce anglicky: Determination of Method for Investigation of Irradiation-induced Steel-concrete Interface Degradation	
Pokyny pro vypracování: Analýza současného stavu jaderných elektráren, rešerše vlivu gama záření na beton biologického stínění, teoretický návrh experimentu soudržnosti a vlivu gama záření, experimentální část návrhu experimentu, numerická modelace metodou konečných prvků	
Seznam doporučené literatury: Hilsdorf, H.K.; Kropp, J.; Koch, H.J. The Effects of Nuclear Radiation on the Mechanical Properties of Concrete. American Concrete Institute Special Publication SP55 1978, 223-251. HOHMANN Brian P., Thomas C. ESSELMAN and James J. WALL: Irradiated Concrete in Nuclear Power Plants: Bridging the Gap in Operational Experience. International Atomic Energy Agency, 2012. IAEA-CN-194-095	
Jméno vedoucího diplomové práce: prof. Ing. Petr Štemberk, Ph.D., D.Eng.	
Datum zadání diplomové práce: 5. 10. 2018	Termín odevzdání diplomové práce: 6. 1. 2019 <i>Údaj uveďte v souladu s datem v časovém plánu příslušného ak. roku</i>
 Podpis vedoucího práce	 Podpis vedoucího katedry

III. PŘEVZETÍ ZADÁNÍ

<i>Beru na vědomí, že jsem povinen vypracovat diplomovou práci samostatně, bez cizí pomoci, s výjimkou poskytnutých konzultací. Seznam použité literatury, jiných pramenů a jmen konzultantů je nutné uvést v diplomové práci a při citování postupovat v souladu s metodickou příručkou ČVUT „Jak psát vysokoškolské závěrečné práce“ a metodickým pokynem ČVUT „O dodržování etických principů při přípravě vysokoškolských závěrečných prací“.</i>	
<u>5. 10. 2018</u> Datum převzetí zadání	 Podpis studenta(ky)

SPECIFIKACE ZADÁNÍ

Jméno diplomanta: Denisa Kavanová

Název diplomové práce: Stanovení metody pro zkoumání degradace rozhraní oceli a betonu způsobené ozářením

Základní část: Rešerše, experiment a numerické modelování podíl: 100 %

Formulace úkolů: Analýza současného stavu jaderných elektráren

Rešerše vlivu gama záření na beton biologického stínění

Teoretický návrh experimentu soudržnosti a vlivu gama záření

Experimentální část návrhu experimentu soudržnosti a vlivu gama záření

Numerické modelování metodou konečných prvků

Podpis vedoucího DP: 

Datum: 26.11.2018

Případné další části diplomové práce (části a jejich podíl určí vedoucí DP):

2. Část: podíl: %

Konzultant (jméno, katedra):

Formulace úkolů:

Podpis konzultanta:

Datum:

3. Část: podíl: %

Konzultant (jméno, katedra):

Formulace úkolů:

Podpis konzultanta:

Datum:

4. Část: podíl: %

Konzultant (jméno, katedra):

Formulace úkolů:

Podpis konzultanta:

Datum:

Poznámka:

Zadání včetně vyplněných specifikací je nedílnou součástí diplomové práce a musí být přiloženo k odevzdané práci. (Vyplněné specifikace není nutné odevzdat na studijní oddělení spolu s 1.stranou zadání již ve 2.týdnu semestru)

DECLARATION

I hereby confirm that I have worked on my master's thesis on my own, just with the advisement of my supervisor prof. Ing. Petr Štemberk, Ph.D., D.Eng.

I declare all the references I have used to write this thesis are stated in the bibliography. I am understood with a usage of this thesis according to the § 60 law no. 121/2000 Sb. (Copyright Act).

In Prague, 4th January 2019

Bc. Denisa Kavanová

ACKNOWLEDGMENTS

Firstly, I would like to take this opportunity to thank everyone who has supported me during my endeavor and has made it possible for me to elaborate this master's thesis.

I would like to emphasize my gratitude to my supervisor prof. Ing. Petr Štemberk, Ph.D., D.Eng. for academical leadership, support and help. I would also like to thank Ing. Josef Fládr, Ph.D. for help with the experimental part of the thesis and Mgr. Yuliia Khmurovska for guidance in the numerical modelling. Lastly, I would like to thank my family for support.

ABSTRACT

The purpose of this thesis is to find a suitable method to measure the steel-concrete bond performance in order to determine the effect of long-term irradiation on the quality of the bond at the steel-concrete interface in reinforced concrete. This thesis consists of three parts. Firstly, the literature review analyzes the theoretical background of irradiation, biological shielding concrete, nuclear reactors and the properties of bond. Secondly, the experimental part focuses on design of the experiment for testing of bond degradation on both irradiated and not irradiated concrete samples with steel reinforcement. Finally, the third part is devoted to numerical modelling of this phenomenon by creating a mathematical model to determine the influence of gamma radiation on the of steel-concrete bond using a non-linear axisymmetric finite element modeling.

KEY WORDS

Nuclear Power Plant, Biological Shielding Concrete, Bond, Nuclear Reactor, License Renewal, Gamma Radiation, Non-linear Finite Element Method, Triangular Finite Elements for Axisymmetric Problems, Material Nonlinearity, Modified Newton-Raphson Method

ABSTRAKT

Cílem této práce je najít vhodnou metodu pro měření soudržnosti ocelové výztuže a betonu tak, aby bylo možné zjistit vliv dlouhodobého ozařování na kvalitu soudržnosti na rozhraní oceli a betonu v železobetonu. Tato práce se skládá ze tří částí. Rešeršní část analyzuje problematiku ozařování, betonu biologického stínění, jaderných reaktorů a vlastností soudržnosti. Experimentální část se soustředí na návrh experimentu pro testování soudržnosti ozářených a neozářených vyztužených betonových vzorků. Poslední, třetí část, se zabývá numerickým modelováním, tedy vytvořením materiálového modelu pro vyjádření vlivu gama záření na soudržnost betonu a oceli pomocí nelineární osově souměrné konečně prvkové simulace.

KLÍČOVÁ SLOVA

Jaderná elektrárna, Beton biologického stínění, Soudržnost, Jaderný reaktor, Obnovení licence, Záření gama, Metoda konečných prvků, Trojúhelníkové prvky pro axisymetrickou úlohu, Materiálová nelinearita, Modifikovaná metoda Newton-Raphson

TABLE OF CONTENTS

Declaration	4
Acknowledgments.....	5
Abstract	6
Key words	6
Abstrakt.....	7
Klíčová slova.....	7
Table of contents	8
List of abbreviations used	11
Introduction.....	12
Motivation.....	12
1 Literature research	14
1.1 Radiation	14
1.2 Radioactivity	14
Alpha radiation.....	15
Beta radiation	16
Electron capture	16
Gamma radiation.....	16
Neutron radiation	17
X-radiation	18
1.3 Attenuation of radiation	19
1.4 Principle of BSC	20
1.5 Nuclear reactors	23
1.5.1 Nuclear fission.....	23
1.5.2 Types of nuclear reactors	23

1.5.3	License renewals	27
1.6	Bond of concrete	28
1.6.1	Anchoring and bond stress	29
1.7	Influence of radiation on BSC degradation.....	30
1.8	Proposal of the bond experiment.....	34
1.8.1	Method.....	34
1.8.2	Irradiation device.....	36
2	Experimental research	38
2.1	Principle of the experiment	38
2.2	Concrete mixture and design.....	38
2.3	Testing procedures	40
2.3.1	Series 1	42
2.3.2	Series 2	44
2.3.3	Series 3	47
3	Numerical modelling	51
3.1	Objective	51
3.2	Axisymmetric elements.....	51
3.3	Derivation of the stiffness matrix.....	53
3.4	Application of the axisymmetric elements.....	54
3.5	Method of modelling the bond layer	54
3.5.1	Lagrange multiplier method – multi-point constraints.....	55
3.5.2	Differentiation of stiffness in the bond layer.....	56
3.6	Nonlinear static analysis	56
3.6.1	Incremental control techniques.....	57
3.6.2	Iterative solution methods	58
3.7	Application of the nonlinear static analysis	60
4	Conclusions	66

Bibliography.....	68
List of figures	72
List of tables.....	75

LIST OF ABBREVIATIONS USED

ACI	American Concrete Institute
BSC	Biological shielding concrete
BWR	Boiling Water Reactor
FBR	Fast Breeder Reactor
FEM	Finite Element Method
GMR	Graphite Moderated Reactor
HWR	Heavy Water Reactor
IAEA	International Atomic Energy Agency
LOCA	Loss-of-coolant accident
LWR	Light Water Reactor
MNR	Modified Newton-Raphson
MPC	Multi-point constraint
MSLB	Main steam line break
NPP	Nuclear power plant
NR	Newton-Raphson
NRC	Nuclear Regulatory Commission
PWR	Pressurized Water Reactor
RIVE	Radiation-induced Volumetric Expansion

INTRODUCTION

Nuclear power plants are aging, and operators would like to prolong their licenses. The world's fleet of operating nuclear power plants (NPP) has been in-service for more than 20 years. In order to support the increasing demand for inexpensive and environmentally friendly power, many plants will be required to operate beyond 40 years, which was the original licensing period for the existing NPPs. Unfortunately, safe performance of shielding concrete structures cannot be guaranteed fully within the twenty years. The available data are not sufficient because testing involving ionizing radiation is very expensive and dangerous. This topic is very challenging and that is exactly my motivation to study it. One of the problems which is yet untouched is the bond at the interface of concrete and reinforcement steel in reinforced BSC and the effect of radiation-induced degradation on it.

MOTIVATION

To protect oneself from ionizing radiation a shield is used, most commonly a concrete one. Concrete is a perfect material for shielding radiation, it combines a relatively low cost, appropriate physical parameters and high durability.

The extension of service life of NPPs is one of the main topics in terms of sustainable energy. The design operating period of nuclear power plants is 30 to 40 years and the average age of operating nuclear power plants has been rising steadily. As of July 2017, it was at 29,3 years, increased from 29 in July 2016, as stated The World Nuclear Industry Status Report [1]. Many of nuclear power plants have already reached their design periods and are still functioning.

In the United States the situation is considered to be even more problematic. In the last 20 years only one new reactor has been launched and only four reactors are under construction now. Therefore, the U.S. reactor fleet continues to age. In June 2017 it had an average age of 37 years and 84 of the 99 operating U.S. units have already received an extension, with another nine applications under NRC (Nuclear Regulatory Commission) review [1]. These belong to the oldest reactors in the world. Some nuclear utilities

envisage average reactor lifetimes of beyond 40 years up to 60 and even 80 years. In Fig. 1 the age distribution of nuclear power plants worldwide can be seen as of July 2017. [1]

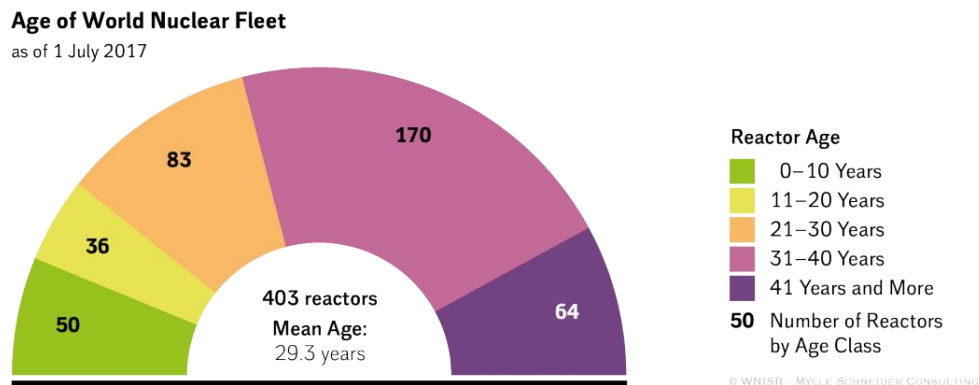


Fig. 1 Age Distribution of Operating Reactors in the World as of June 2017 [1]

The service life of these NPPs could be extended by a license renewal for additional 20 years issued by the U.S. Nuclear Regulatory Commission. It is understandable that the operation life extensions are preferred to the shutdown of the NPP due to the demanding dismantling of the shutdown nuclear power plant which also entails large expenditures for the operator. Today's NPPs are much more expensive and problematic to build than for example in the 1990s, due to the rise of cost of workforce and material. New safe guidelines have been issued following the Fukushima disaster in 2011, which resulted in increase of prices and time-to-build of power plants. However, improved knowledge of the performance of irradiated concrete is required to form a technical basis for long term operation (operation to 80+ years) of nuclear plants around the world. Therefore, the object of this thesis is to design an experiment, which will determine the influence of long-term gamma irradiation on the bond of reinforced biological shielding concrete (BSC).

1 LITERATURE RESEARCH

1.1 Radiation

The most common use of shielding concrete can be found in nuclear power plants, particle accelerators and hospitals. All of these environments have one thing in common – radiation. Even everyday visible light also belongs to radiation, but the most dangerous kind to humans is ionizing radiation, which has a high enough energy to ionize atoms and molecules. Ionizing radiation can be of a different essence, either an electromagnetic radiation of photons, or a current of subatomic particles – nuclei, electrons, positrons, neutrons.

1.2 Radioactivity

Big nuclei containing a large number of protons are naturally unstable and fall apart to lighter elements. This phenomenon is called natural radioactivity. The heaviest isotope able to stay stable is lead ($^{207}_{82}\text{Pb}$), all heavier elements are radioactive – for example radon, uranium or thallium. The decays follow known decay chains. Three main decay chains (or families) are observed in nature, commonly called the thorium series, the radium or uranium series, and the actinium series, representing three of four main classes. These three classes end with different, but stable isotopes of lead. The fourth one, the neptunium series, is artificially produced and ends with an isotope of thallium. The actinium series can be seen in Fig. 2. [2]

The decay can be followed by one of the three types of radiation – α (helium nuclei), β (electrons) and γ (photons), which is part of the electromagnetic spectrum. Some elements can undergo either an alpha or beta decay, these elements create different branches of the decay chains. In addition to the alpha or beta particles emitted as a result of the decay of a parent isotope, most of the daughter isotopes also emit gamma rays. [3]

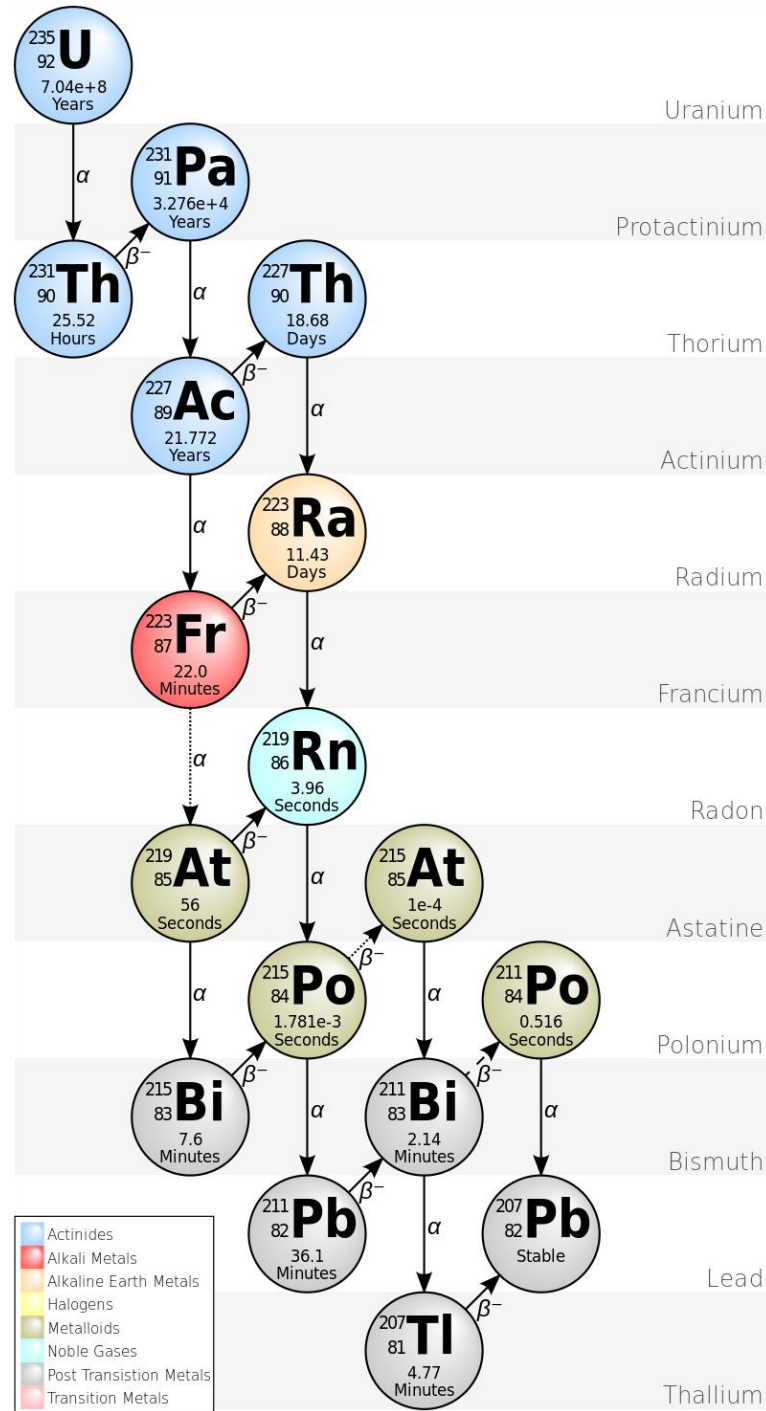


Fig. 2 The Actinium Series [2]

Alpha radiation

It consists of helium nuclei – hellions. Their energy lies between 4 MeV and 9 MeV. The range of these particles is very small since they very quickly lose their energy by ionizing the surroundings. In gases it is estimated to be a few centimeters, in liquids and solids just fractions of millimeters. Ergo it is not necessary to shield oneself from this

type of radiation. The example of an element emitting alpha radiation is radon, uranium or americium.

Beta radiation

It is a current of fast electrons (β^-) or positrons (β^+) with a high range of energies. β^+ exists mainly with manmade radionuclides. When the beta particles go through mass three events can occur: elastic dispersion in a nucleus or in an orbital (mainly with slow electrons), ionization and a loss of energy (the power of ionization is lower than with alpha) or hinder X-radiation of fast electrons – when they slow down, X-rays are emitted. Beta radiation is rather harmless, but the X-rays are much more penetrable. If the beta is absorbed by a high-density substance, the energy of hinder X-rays is higher, which is why it is best to shield beta radiation with light element e.g. plexiglass. The particles of beta are lighter and smaller compared to alpha and therefore can travel a longer distance with smaller losses of energy. The range is approximately 8 meters in air, 1 centimeter in water and 4 millimeters in aluminum. When β^+ – positrons – go through a mass, and it is combined with an electron, the so-called annihilation occurs resulting in two photons. This means every beta radiator and its container is simultaneously a source of a penetrating photon radiation. An example of β^- is cobalt and cesium, an example of β^+ is sodium and carbon.

Electron capture

When a nucleus contains an extra proton, it captures one electron from his K-orbital and the proton changes to a neutron. The empty spot in the K-orbital is filled by an electron from a higher orbital and the extra energy is emitted in a form of a photon. The example of this is zinc or cadmium.

Gamma radiation

It is an electromagnetic radiation consisting of photons with a very small wavelength (10^{-11} to 10^{-13} m). It originates when a nucleus is changing from a high-energy to a low-energy state and is getting rid of its excitation energy. It is usually accompanied by alpha or beta radiation. The best way to shield gamma is heavy materials. When gamma goes through a mass the photons release electrically charged particles, which ionize and excite the environment. Three kinds of interaction can follow:

Part I: Literature research

- Photoelectric effect – the photon transfers all its energy to an electron and releases it from the atom. The empty spot is filled with an electron from a higher orbit and a photon is released.
- Compton dispersion - the photon transfers a part of its energy to a weakly bound electron, which begins to move. The photon with a lower energy changes then consequently its direction.
- Creation of an electron-positron pair – if the photon has a higher energy than 1,02 MeV it can be absorbed and create an electron-positron pair. Eventual excess of energy rises the kinetic energy of the newly created pair.

The penetration force of alpha, beta and gamma radiation in the human body can be seen in Fig. 3. [4]

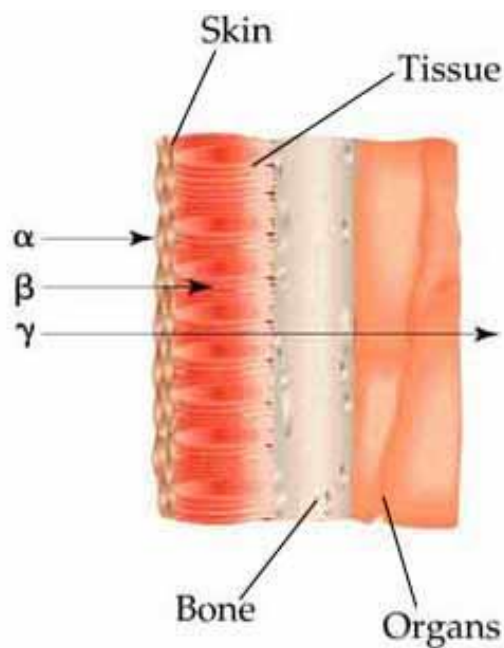


Fig. 3 The Penetration Force of Alpha, Beta and Gamma Radiation in the Human Body [4]

Neutron radiation

Neutrons are present at nuclear reactions and at a spontaneous atom split. They behave according to their energy:

Name		Energy
cold	slow	< 0,002 eV
thermal		0,002 – 0,5 eV
resonance		0,5 – 1000 eV
intermediate		1 – 500 keV

Part I: Literature research

fast	0,5 – 10 MeV
very fast	10 – 50 MeV
ultrafast	> 50 MeV

The sources of neutrons can be divided into radionuclide sources, neutron generators and nuclear reactors, which work on the principle of spontaneous fission. Together with gamma they belong to the most dangerous kinds of radiation. The interaction of neutrons with a mass differs from the previous. Since neutrons have no electrical charge, nuclear instead of electrical forces apply. Most importantly can occur:

- Elastic dispersion – change of the direction of the neutron and transferring certain energy to the proton of the mass. The element most capable of to slowing down neutrons is hydrogen.
- Neutron capture – neutron is absorbed by the nucleus
- Non-elastic dispersion
- Fission of nuclei

Multi-component shielding is often used. Light materials to slow down neutrons (water, paraffin), other to capture them (boron, cadmium). Sometimes also a heavy material is needed to shield the gamma from neutron capture.

X-radiation

It is an electromagnetic radiation with a small wavelength (10^{-9} to 10^{-13} m). It originates when fast electrons slowdown (hinder) in heavy metals. The properties and interactions are of the same principle as with gamma radiation. The source of the electrons (β^-) is called a cathode, the metal an anode. Two kinds of X-ray can be distinguished: hinder and characteristic. Hinder radiation is founded on the loss of the kinetic energy of electrons and is independent of the material of the anode. Characteristic radiation originates when the electron enters the orbital of the anode. In certain conditions the cathode electron can smash out an anode electron from its route. Its spot is filled with one from a higher energetic surface and the extra energy is irradiated in form of X-rays. This kind of X-ray is dependent of the anode material.

The above-mentioned kinds of radiation and their shielding methods are depicted in Fig. 4. [5]

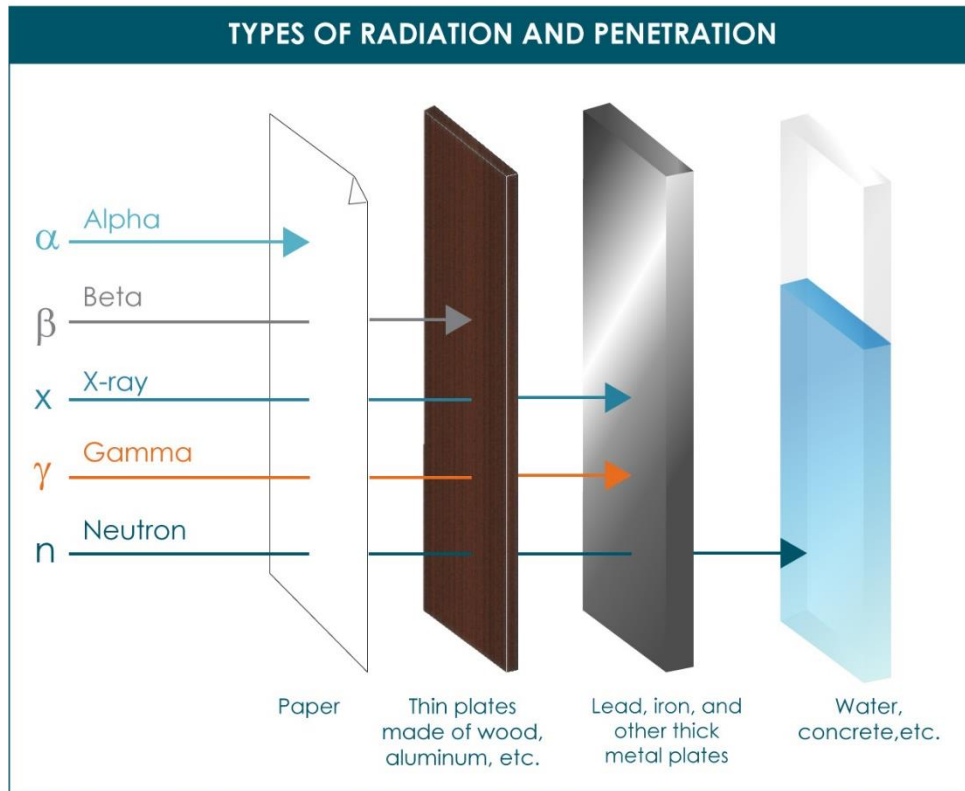


Fig. 4 Diagram of Different Kinds of Radiation and Shielding Options [5]

1.3 Attenuation of radiation

When all of the above-mentioned radiation goes through an environment that contains mass it loses energy and therefore is absorbed. Particle flow density of a small stream of monoenergetic radiation decreases in a layer of material accordingly [2]:

$$\varphi = \varphi_0 e^{-\mu d}$$

where

φ_0 – the original particle flow density

φ – the particle flow density after the passage through a layer of material of thickness d

μ – linear absorption coefficient [m^{-1}]

This absorption law can be further transcribed:

$$\varphi = \varphi_0 e^{-\mu_m \rho d}$$

where

Part I: Literature research

$$\mu_m = \frac{\mu}{\rho} \text{ – weight absorption coefficient [kg}^{-1}\cdot\text{m}^2\text{]}$$

ρ – density of the absorbing medium [kg.m⁻³]

$\rho \cdot d$ – area density of the material layer [kg.m⁻²]

The easiest way to imagine the permeability of radiation of a material is the half-value layer ($d_{1/2}$). It is defined as a thickness of a layer which reduces the particle flow density to half. Seven half-value layers will reduce the radiation level approximately 100 times, and ten half-value layers will reduce the radiation level by a factor of 1000 [6]. The half-value layer and the linear absorption coefficient are bounded together by a formula:

$$d_{1/2} = \frac{0,693}{\mu}$$

1.4 Principle of BSC

In nuclear reactors it is necessary to shield oneself from two kinds of dangerous radiation – gamma and neutron radiation. Concrete is the most suited material for biological shielding thanks to its excellent mechanical properties, chemical composition, economic availability and relatively low-cost construction.

Gamma radiation is absorbed by interactions with electrons of heavy and large atoms, but neutron radiation interacts with the nuclei of atoms. Neutrons in the reactor move at energy levels from 0.1 to 14 MeV, while those with the highest energy also lose their energy through inelastic collisions with heavy atoms. The slower ones lose their energy efficiently by collisions with light atoms, preferably with hydrogen, which is similar in weight to the neutron. However, the material that absorbs neutron radiation can be the source of secondary gamma radiation, which complicates the shielding problem further. The ability of the material to prevent this secondary radiation is called a nuclear cross section [m²], as boron is often added to the shielding material due to its high nuclear cross section area and emits almost no secondary radiation. [7]

Effective shielding material is therefore a combination of a heavy material with a lightweight one and possibly a high nuclear cross section. These requirements exactly match the composition of concrete in which the chemically bound water serves as a lightweight additive. Problems with concrete can be as follows:

Part I: Literature research

1. The density of conventional concrete 2500 kg/m^3 is quite low and requires very wide shielding walls; some reactors require a thickness of more than 2700 mm.
2. During the operation of the nuclear reactor, the concrete can be dried by the heat, because the temperature in the reactor is usually around 60°C . Loss of water reduces its resistance to neutron radiation, as well as its density, and therefore resistance to fast neutrons and gamma rays.
3. The unanswered question that remains is the impact of radiation on the quality of concrete over the years. The long-term behavior of the concrete has not been sufficiently explored yet, but currently there are licenses for nuclear power plants being prolonged around the world. The impact on the cohesion between concrete and reinforcement is also unknown. The influence of thermal stress may be masked in experiments due to radiation, it is difficult to strictly separate these two factors.

The solution for improving the properties of BSC can be following:

1. Increasing the density of concrete - using heavy aggregates, minerals with density greater than 3000 kg/m^3 . Natural materials that can be used are iron ore, barite, limonite, goethite, hematite, magnetite and ilmenite. Artificially made options are ferrophosphorus and iron or steel inclusions. This method is the most common in practice. An example of iron ore can be seen in Fig. 5. [8]
2. An increase in the proportion of hydrogen in the material - can be done by increasing the proportion of water using an aggregate with high level of humidity and aggregate capable of maintaining humidity at higher temperatures (such as serpentinite) or by using special cements that absorb more water than Portland cement. In theory, a compound with lighter atoms than water, such as deuterium, helium, beryllium and carbon, can be added to the material, but this is not used often in practice for economic and practical reasons.
3. Addition of a material with high nuclear cross section to absorb slow neutrons and prevent secondary gamma radiation - it can be boron, cadmium, cobalt, mercury or silver. In practice, the addition of these

Part I: Literature research

substances to the concrete mixture is not used, but limonite and goethite have a high boron content. [7]



Fig. 5 Example of Iron Ore [8]

The properties of heavy aggregates can be found in the following Tab. 1. [9]

Tab. 1 Properties of Heavy Aggregates

Type of aggregate	Fixed-water, percent by weight	Aggregate particle density [kg/m ³]	Aggregate bulk density [kg/m ³]	Concrete density [kg/m ³]
Goethite	10-11	3 400-3 700	2 080-2 240	2 880-3 200
Limonite	8-9	3 400-4 000	2 080-2 400	2 880-3 360
Barite	0	4 000-4 600	2 320-2 560	3 360-3 680
Ilmenite	*	4 300-4 800	2 560-2 700	3 520-3 850
Hematite	*	4 900-5 300	2 880-3 200	3 850-4 170
Magnetite	*	4 200-5 200	2 400-3 040	3 360-4 170
Ferrophosphorus	0	5 800-6 800	3 200-4 160	4 080-5 290
Steel punchings	0	6 200-7 800	3 860-4 650	4 650-6 090

*Aggregates may be combined with limonite to produce fixed-water contents varying from 0.5% to 5%.

1.5 Nuclear reactors

1.5.1 Nuclear fission

Inside the nuclear reactors a chain reaction occurs. Unstable uranium 235 nuclei (for example, most common type of fuel is in form of uranium-dioxide UO_2) are impaired by the impact of slow neutrons and collapse while releasing energy into barium and krypton or lanthanum and bromine atoms. At the same time, two to three other fast neutrons are released from the core, which, after their slowing down, ensure the continuation of the reaction and the fission of other uranium atoms. Neutrons are slowed down using so-called moderators - such as graphite, light water H_2O or heavy water D_2O (deuterium). Neutron absorbers, such as boric acid solution that is added to the primary circuit coolant water, are used to regulate the reaction and prevent exponential growth of the number of fissions. Another way to absorb neutrons is to insert cadmium rods into the nuclear reactor or change the insertion depth. [10]

1.5.2 Types of nuclear reactors

According to the Institute for Energy and Environmental Research (IEER's report [11]), nuclear reactors can be divided into three categories based on their purpose. Firstly, there are civilian reactors, which provide energy for the peoples of the world, secondly it's military reactors, whose main purpose is creating materials that can be used as a nuclear weapon and thirdly there are research reactors used for nuclear research and experimentation, developing weapons or new energy production technology, training purposes and producing radio-isotopes for medicine and research. Military applications also include nuclear engines – submarines and are related to thermal rockets for spacecraft technology. The fuel which is used, its chemical composition (for example the percent composition of uranium U_{235} isotope and uranium U_{238} isotope), type of coolant and other details which are very important to the operation of the reactor depend on the specifics of the reactor design. Natural uranium is 99,284 % U_{238} isotope, the enriched uranium is a fuel, where the percent composition of Uranium U_{235} has been increased through the process of isotope separation. [12]

The following Tab. 2 shows the parameters of the main types of nuclear reactors – Light Water Reactor (LWR), Heavy Water Reactor (HWR), Graphite Moderated Reactor (GMR), Fast Breeder Reactor (FBR). [12]

Tab. 2 Types of Nuclear Reactors – Part 1

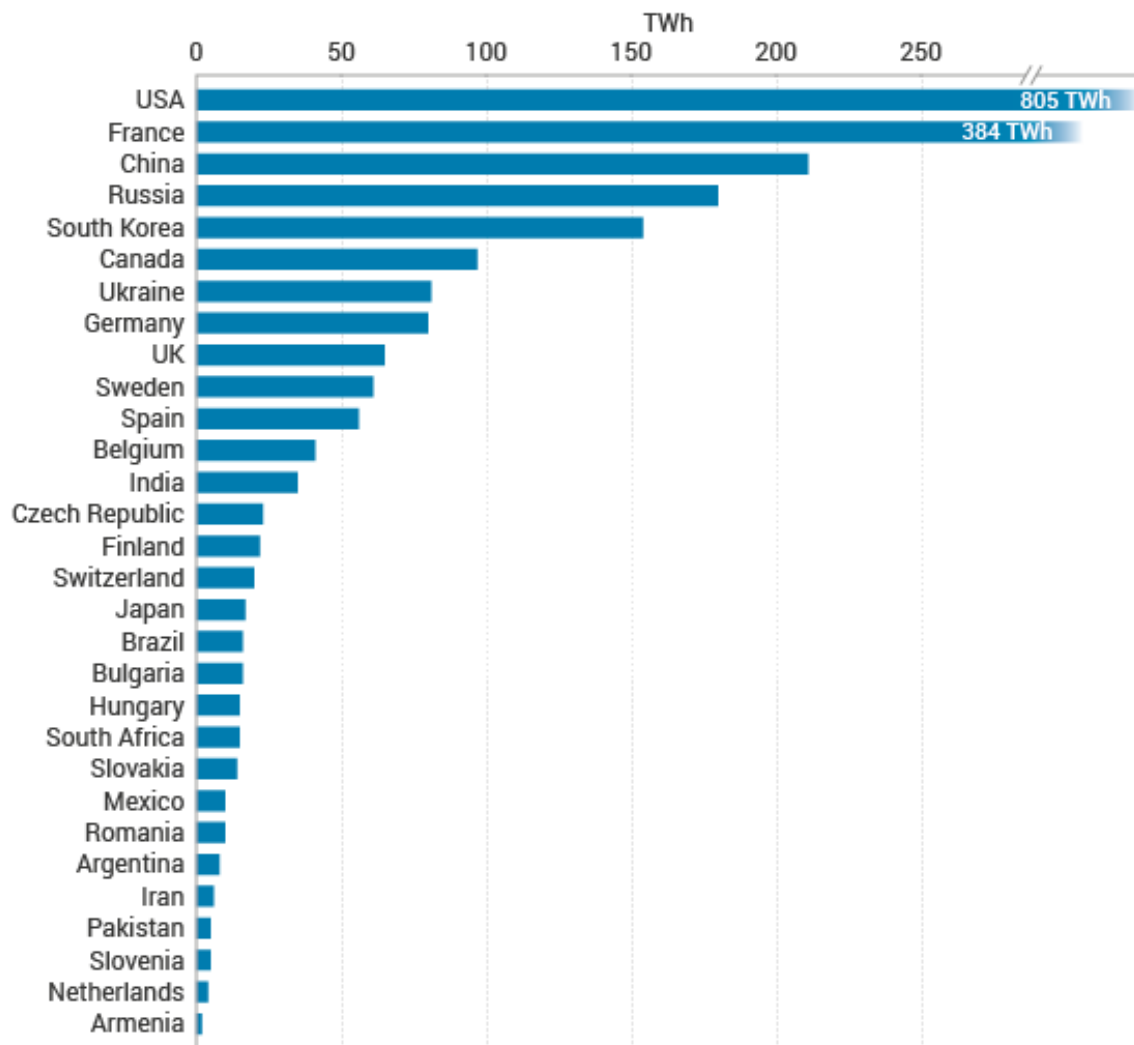
Reactor Type	Light Water Reactor		Heavy Water Reactor
	Boiling Water Reactor	Pressurized Water Reactor	
Purpose	electricity	electricity; nuclear powered ships (U.S.)	electricity; plutonium production
Coolant Type	water (H ₂ O)	water	heavy water (deuterium oxide, D ₂ O)
Moderator Type	water	water	heavy water
Fuel-Chemical Composition	uranium-dioxide (UO ₂)	uranium-dioxide	uranium-dioxide or metal
Fuel-Enrichment Level	low-enriched	low-enriched	natural uranium (not enriched)
Comments	steam generated inside the reactor goes directly to turbine	steam is generated outside the reactor in a secondary heat transfer loop, type VVER in Russia and Czech Republic	used in Canada: called “CANDU” – “Canadian Deuterium Uranium”; Also used in Savannah River Site reactors (metal fuel at SRS)

Tab. 2 Types of Nuclear Reactors – Part 2

Reactor Type	Graphite Moderated Reactor		Fast Breeder Reactor
	Gas Cooled	Water Cooled	Liquid Metal (most common type of breeder)
Purpose	electricity; plutonium production	electricity; plutonium production	electricity; plutonium production
Coolant Type	gas (carbon dioxide or helium)	water	molten, liquid sodium
Moderator Type	graphite	graphite	not required
Fuel-Chemical Composition	uranium-dicarbide (UC ₂)	uranium dioxide (RBMK) or metal (N-reactor)	plutonium dioxide and uranium dioxide in various arrangements
Fuel-Enrichment Level	slightly enriched, natural uranium	slightly-enriched	various mixtures of plutonium-239 and uranium-235
Comments	used in Britain, and France (e.g.: AGR, MAGNOX)	used in former Soviet Union, e.g. Chernobyl (RBMK); N-reactor at Hanford	breeder reactors are designed to produce more fissile material than they consume. Monju; Phenix

Part I: Literature research

The first commercial NPPs started operating in the 1950s. Nowadays there are about 450 nuclear power reactors in 30 countries worldwide, which generate around 11% of the world's electricity. 60 other reactors are under construction and 150-160 are in a phase of planning. Besides these, there are 225 research reactors in 50 countries, which are used for research and production of medical and industrial isotopes. USA has the biggest nuclear electricity production, followed by France and China, see Fig. 6. On the other side of the spectrum stands Germany, who has shut down all of their NPPs following the Fukushima nuclear disaster. [13]



Source: IAEA PRIS Database

Fig. 6 Nuclear Electricity Production Worldwide, April 2018 [13]

The biological shielding concrete is present around the reactor vessel, as can be seen in Fig. 7. [14] It is a thick layer of concrete exceeding 60cm. In VVER nuclear reactors it has only a shielding function, but for example in case of BWRs with MARK I

containment it has also a bearing function [15]. This BSC can be reinforced, but the effects of the reinforcements are still unknown.

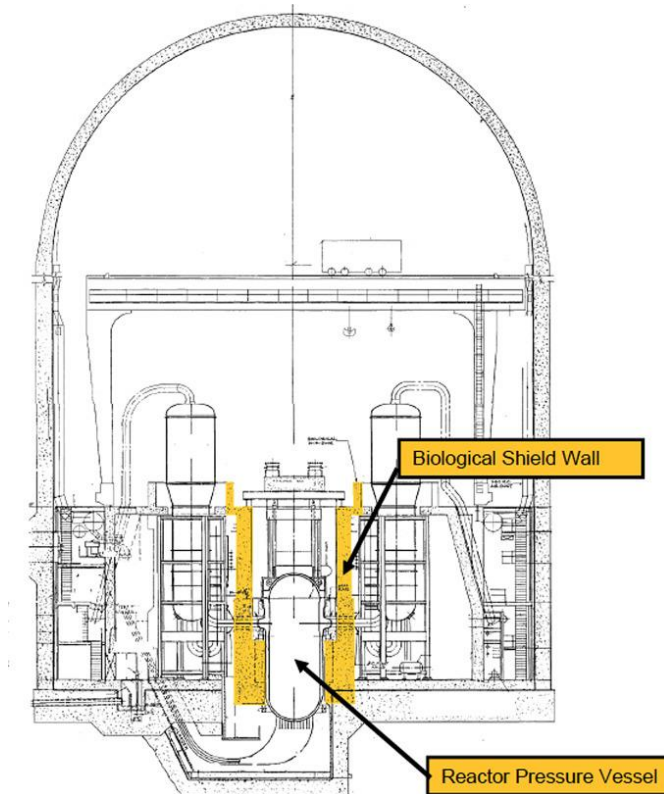


Fig. 7 Location of BSC in a Nuclear Reactor [14]

A nuclear vessel resides in the heart of the nuclear reactor, the whole building is surrounded by a concrete shell called containment, usually lined with steel. It is the final barrier to prevent release of radioactive material in case of an accident (for example LOCA – loss-of-coolant accident) with pressure-suppression systems. Other functions are to condense steam from primary coolant and to contain it inside the building and protection from external events.

These are the main types of containment buildings [16]:

- Full pressure dry containment (PWR) – steel or concrete shell, during normal operation a prescribed negative pressure is maintained
- Full pressure double wall containment (PWR) – steel or concrete shell with a secondary concrete confinement building, same principle as full pressure dry containment only with extra layer of protection
- Bubbling condenser containment building (PWR) – uses a concept of suppression pool(s) in which the high-pressure steam is directed to

following a LOCA or MSLB (main steam line break), the submerged pools suppress the pressure – the steam is condensed

- Ice condenser containment building (PWR) – uses a system of ice chambers containing baskets of ice, which work the same way against LOCA or MSLB as suppression pools, only more effective as they can contain more heat (latent heat of fusion)
- BWR containment buildings – more compact than PWR containments, since there is no steam generator. Major designs are the Mark I, Mark II and the Mark III. A BWR containment consists of a drywell, which houses the reactor, the suppression pool in a form of a surrounding ring or a ‘wet well’ and the containment envelope.
- Pressurized containments in heavy water reactors – unlike an LWR, HWR containments are accessible and ventilation is needed. Some HWR use single unit suppression so following systems are in place: concrete containment is prestressed and post-tensioned, there is a tank around the building and a powerful spray system and a long-term containment cooling system. Some units use a vacuum building which is connected to the containment building and works as a pressure suppression system.

1.5.3 License renewals

The license renewal is a long and demanding process that includes both legal and engineering reviews, evaluation of engineering infrastructure and safety checks of generating hardware. In Fig. 8, NPPs in USA that have been granted a license renewal by the year 2013 can be seen, in total two thirds of them [17]. Concrete is the most common used building material in the nuclear power plants and concrete plays an important role in ensuring their safety. That is the reason why about 80% of Pressurized Water Reactors (PWRs) utilized primary containments are made of concrete. Nowadays an extensive research effort is focused on concrete performance in irradiated environment.

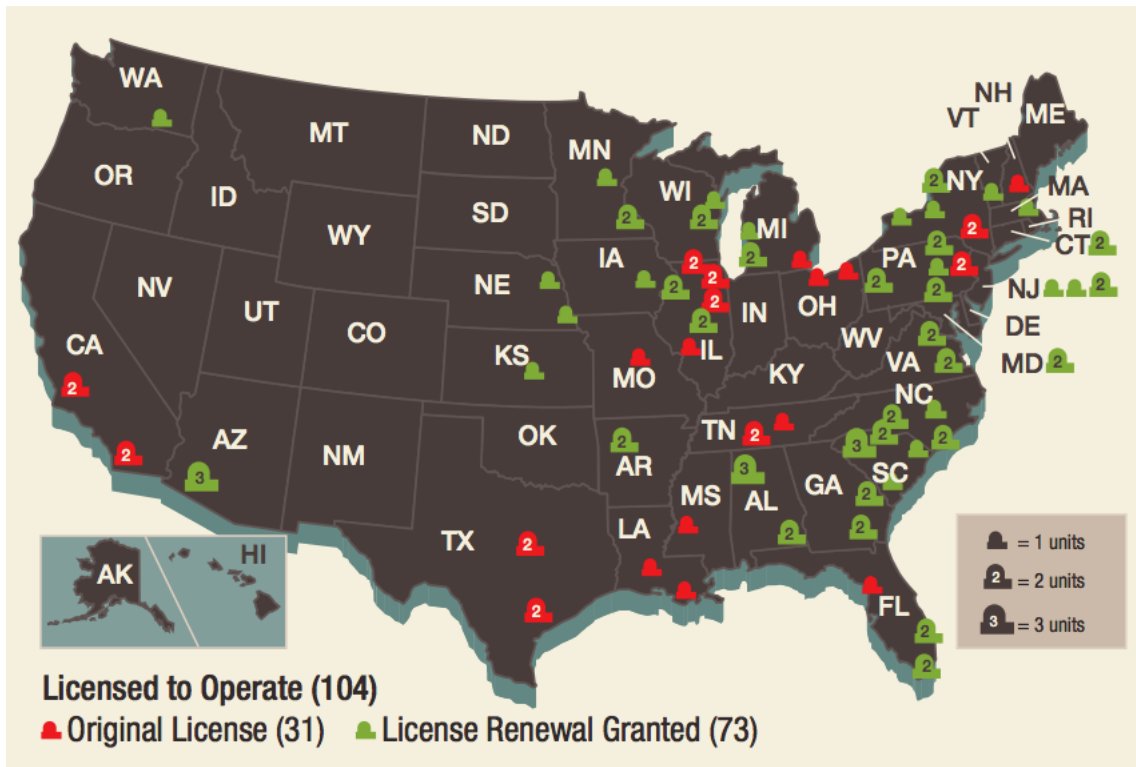


Fig. 8 License Renewals Granted for Operating Nuclear Power Reactors in USA as of 2013 [17]

Many other countries appoint no defined time limits on operating licenses. In France, where the country's first operating Pressurized Water Reactor (PWR) started up in 1977, reactors must undergo thorough inspection and testing every decade evaluating strict safety requirements. The French nuclear reactors have operated for 32.4 years on average, and the oldest have completed the process with the French Nuclear Safety Authority (ASN) evaluating each reactor before allowing a unit to operate for more than 30 years. The assessments of NPPs in France are however years behind schedule. They could then operate until the age of 40 years, which is the limit of their initial design age, same as most other countries operating NPPs. [1]

1.6 Bond of concrete

The basic conditions of static interaction of concrete and steel reinforcement in a reinforced concrete construction are:

1. Bond between concrete and reinforcement rebars
2. Same value of the coefficient of thermal expansion of concrete and steel
3. Protection of reinforcement against corrosion and acid environment, the concrete provides an alkaline environment

1.6.1 Anchoring and bond stress

The anchoring of longitudinal reinforcement must securely transfer the forces from the reinforcement to the concrete, it must prevent the formation of cracks and prevent the concrete from being split off, if necessary add shear reinforcement.

The parameters of bond are influenced by a number of things, for example the quality of steel, quality of concrete, which has to contain enough cement and an appropriate proportion of other mixture ingredients. Good coverage of the rebar by the mixture must be secured to ensure full interaction of the bond. Typically, the upper reinforcement in a plate face this problem and there is a smaller bond measured than in the lower layer of the reinforcement.

The steel rebars cannot be contaminated with substances negatively influencing the cement hydration, e.g. lubricating substances. On the contrary a slightly rusted rebars are welcome, because the hydrating cement penetrates into the unevenness on the surface of the reinforcement and the bond is better than with using a complete smooth rebars. That is the reason behind using ribbed rebars, which can be seen in Fig. 9. [18]

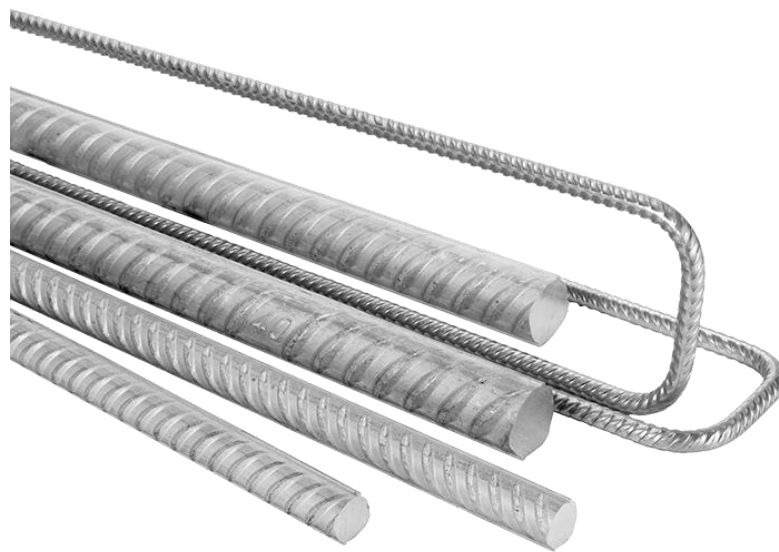


Fig. 9 Ribbed Reinforcement Bars [18]

Even though the ASTM and EU norms differ in specific formulas, the basic principle of ensuring bond remains the same across the globe: The force needed to rip out the reinforcement bar from concrete has to be greater than the force needed to break the reinforcement bar as can be seen in the following formula:

$$F_b \geq F_t \quad (1)$$

where

F_b – rip out force of the rebar [N]

F_t – rupture force of the rebar [N]

When loading the specimen, the tangential stress is not uniform, but we simplify the problem and assume a uniform stress along the concrete-steel zone such as:

$$\tau_s = \frac{F}{u \cdot l_a} \quad (2)$$

where

τ_s – tangential stress [Pa]

F_t – rupture force of the rebar [N]

u – circumference of the rebar [m]

l_a – length of the anchorage [m]

From equations (1) and (2) we can derive the necessary anchorage length, maximum bond stress [Pa] and steel tensile strength [Pa] have to be provided.

Maximum bond stress can be calculated based on the diameter of the rebar, compressive strength of the concrete and other coefficients depending on the quality of the conditions of the concreting and geometry. The primary and design anchorage lengths can be modified by coefficients of the diameter of the rebar, stress of the steel, cover layer and shape of the rebar. When designing the cover layer of concrete one of the requirements is the bond of the concrete. [19]

1.7 Influence of radiation on BSC degradation

Despite concrete being used both in the primary and secondary containment structures, only a limited amount of original research on the topic of the long-term effects of irradiation on concrete mechanical properties and structural bearing capacity of

Part I: Literature research

biological shield walls and vessel support structures is available. The prolongation of licenses of NPPs could be in conflict with a change in the physical, mechanical, or chemical properties of concrete structures that are exposed to chronic radiation.

Since aggregate materials are found in sand and gravel that is typically secured from a local quarry during the construction of a NPP and aggregate raw materials typically account for approximately 75% of the total concrete volume, a methodology for characterizing irradiated concrete must be able to account for this level of variability in order to determine of the effect of irradiation on concrete.

The attenuation of radiation results in the generation of heat, which causes higher than expected stresses because of the temperature gradient across the concrete. There is also a problem with retaining water in case of gamma radiation. A method isolating the effects of radiation and the effects of elevated temperature is needed to provide clear results, but the influence of radiation and temperature on concrete is very difficult to isolate experimentally, because both occur simultaneously. [20]

Hilsdorf et al. wrote a publication in 1978 [21] describing the effects of nuclear radiation on the mechanical properties of concrete, which is an important foundation of the field of nuclear power. Hilsdorf collected formerly published experimental data on the effect of nuclear radiation on concrete, specifically focusing on properties such as compressive strength and tensile strength of concrete, temperature, and radiation dose.

Hilsdorf summarized the available data to show the impact of neutron irradiation on compressive strength as can be seen in Fig. 10 [21]. Hilsdorf concluded that neutron radiation with a fluence of greater than 1×10^{19} n/cm² (neutron per square centimeter) may have a negative effect on concrete strength and modulus of elasticity. Additionally, the data Hilsdorf based his analysis on showed that in the lifespan of a nuclear reactor the neutron radiation fluence may exceed 5×10^{19} n/cm². Thermal coefficient of expansion, thermal conductivity and shielding properties of concrete are little affected by radiation.

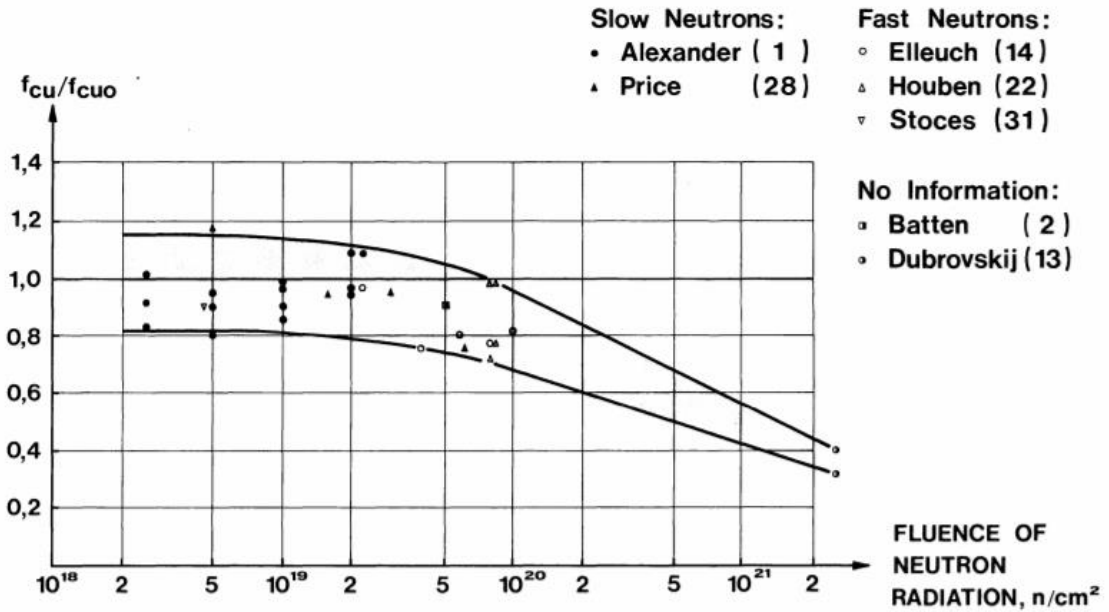


Fig. 10 Compressive Strength of Concrete Exposed to Neutron Radiation f_{cu} Related to Strength of Untreated Concrete f_{cuo} [21]

Radiation damage is mainly caused by mesh defects in the aggregates which are then subject to a volume increase. This results in a volume increase of concrete structures. This phenomenon is called the Radiation-induced volumetric expansion or RIVE and the effect together with cement shrinkage, which can also be observed, can be seen in Fig. 11 [21]. Different aggregates show different resistance against irradiation which makes the selection of the aggregate the most important parameter in the design of a BSC.

The publication shows a decreasing dependence of compressive and tensile strength of concrete exposed to gamma radiation on the radiation dose. If we take into account the average dose rate of a research nuclear reactor at the walls, the value is about 200 Gy/h [22], we get a total of 7×10^7 Gy (7×10^9 rad) in the 40-year life span of a NPP. This amount of gamma radiation doesn't affect the concrete much, but twice as long life of the NPP, as planned in some license renewals, could mean significant damage to the concrete and decrease of compressive and tension strength, as can be seen in Fig. 12 [21].

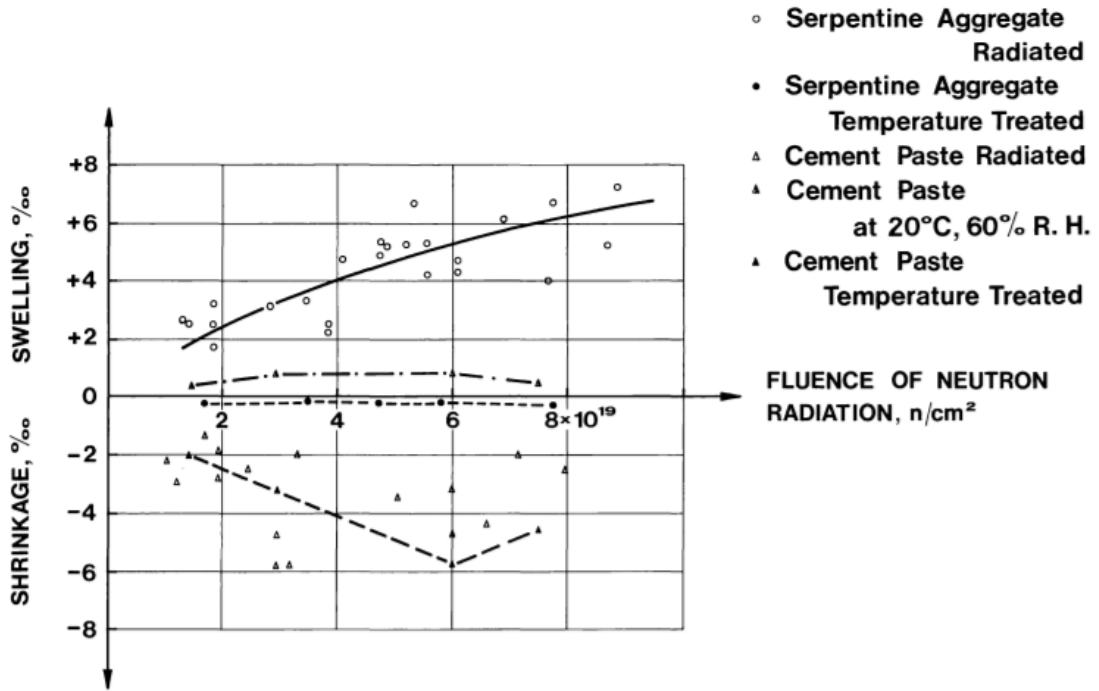


Fig. 11 Volume Change of Aggregates and Hardened Cement Paste During Radiation with Fast Neutrons [21]

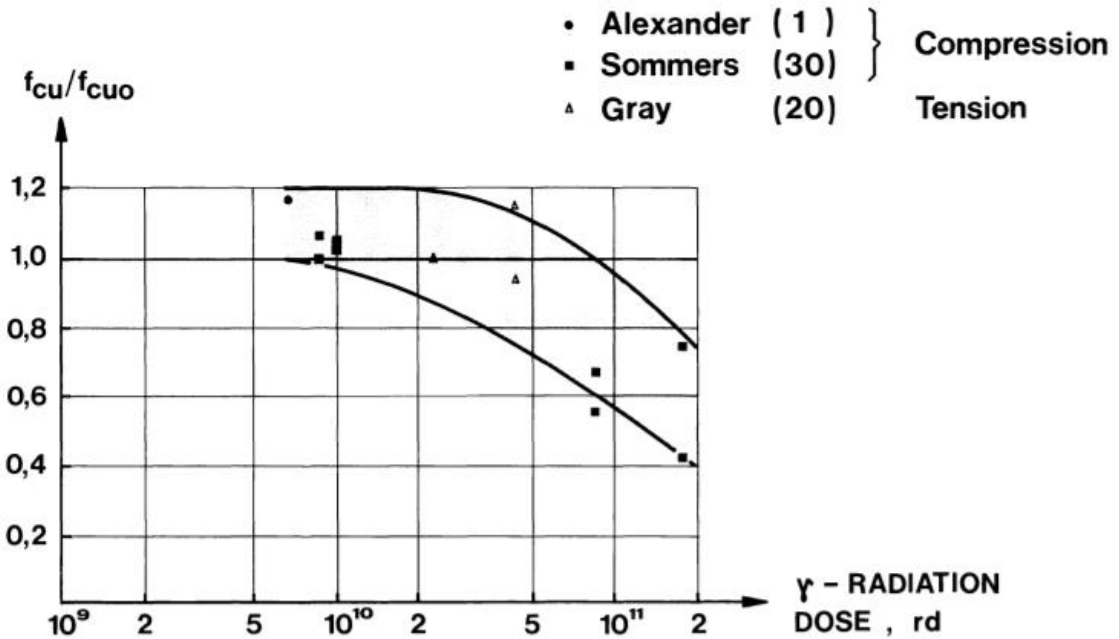


Fig. 12 Compressive and Tensile Strength of Concrete Exposed to Gamma Radiation f_{cu} , Related to Strength of Untreated Concrete f_{cu0} [21]

Recently, O. Kontani and colleagues concluded that the test conditions from some of the experiments on which Hilsdorf based his conclusions were not representative of the typical operating history of a commercial nuclear reactor, and thus may not be

applicable. In commercially operating nuclear power plants, temperatures in the reactor building are normally kept below 65 degrees Celsius. Some of the data points with fluence levels between 3×10^{19} n/cm² and 1×10^{20} n/cm² included in Hilsdorf's review were obtained from aluminous cement samples under irradiated temperatures between 150-200°C [23].

After Hilsdorf's paper, very little experimental research was performed on the long-term effects of radiation exposure on concrete. As there is a lack of independent research on the topic of irradiated concrete, most governmental documents, both in the United States and internationally, use the fluence values determined by Hilsdorf as their values of thresholds for maximum dose of neutron and gamma radiation. Specification ACI 349.3R-02 for the American Concrete Institute (ACI), states that critical cumulative fluence levels for a whole period of a NPP life cycle are 1×10^{25} neutrons/m² (1×10^{21} neutrons/cm²) and 10^{10} rad (gamma dose). A limit for preventing any lifetime radiation-related degradation has been recommended at 1×10^{17} neutrons/m² (1×10^{13} neutrons/cm²) fluence [24]. Both Nuclear Regulatory Commission [25] and IAEA [26] documents refer still use the values determined by Hilsdorf as well.

Since approximately 2002, more publications on the topic of concrete irradiation effects have been written. Use of numerical modeling has increased and this method has been used by many researchers globally to investigate the effect of irradiation on concrete. However, in order for these computer models to be validated and benchmarked, more experimental data is needed to determine actual fluence levels and changes in material properties. An effective source of irradiated concrete could be found in shut down and decommissioned NPPs. A primary requirement for irradiated concrete cores is that they include both an irradiated (section closest to the reactor vessel) part of the core and unirradiated (material near the outside diameter of the biological shield) part of the same core so that the effects of irradiation can be clearly identified. A united method for clear and uniform testing and characterizing of the core samples removed from decommissioned NPPs will aid in overcoming variability in the gained data.

1.8 Proposal of the bond experiment

1.8.1 Method

The proposed experiment was chosen to be a push-in experiment with a bond stress-slip relationship, which is virtually similar to a pull-out test. This experiment will

be performed with irradiated and non-irradiated specimens and the results will be compared to find out the influence of gamma radiation on the bond of reinforced concrete. The details such as shape of the used specimen and mixture design are described in the Experimental research part of this thesis.

One of the major problems in reinforced concrete bond research is the absence of a generalized method for measuring and determining bond strength. Most researchers use pull-out tests that are commonly adopted in reinforced concrete bond studies. In general, bond action is represented by the bond stress-slip relationship.

As shown in Fig. 13 [27], the stress transfer mechanisms, which refer to the bond action, are usually expressed by the bond stress-slip relationship obtained from pull-out tests. The bond actions are comprised of an adhesive bond, a frictional bond, and a shear bond. In the case of deformed (ribbed) bars, the bond resistance capacity is mainly determined by the mechanical interlocking action.

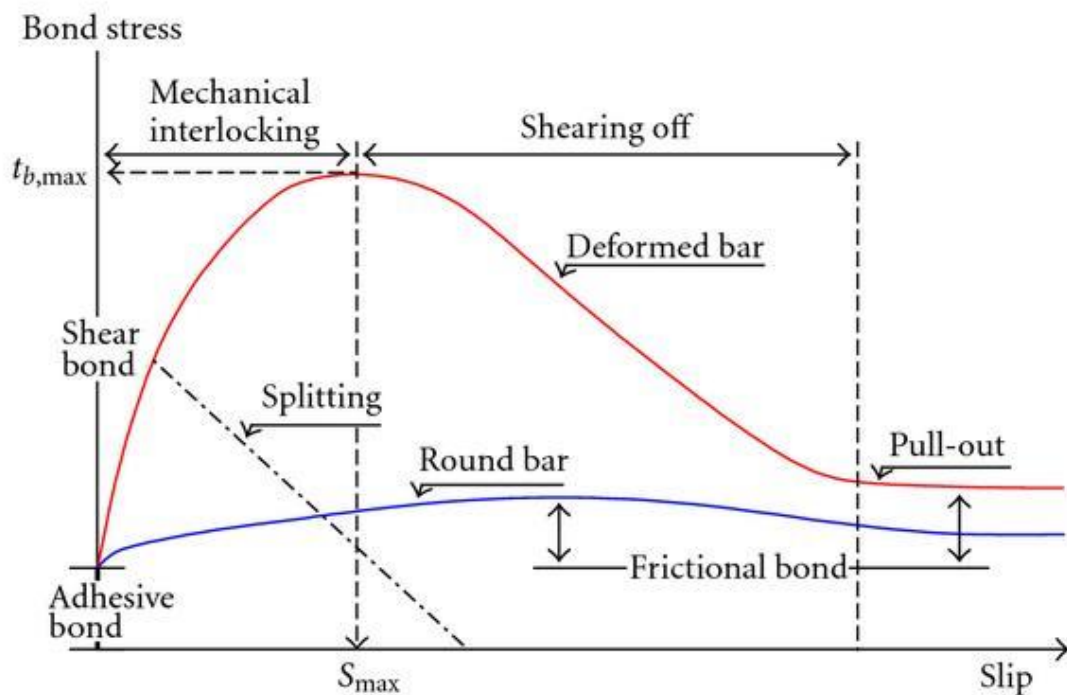


Fig. 13 Bond Stress-slip Relationship [27]

Generally, test methods which are used to measure bond stress and slip can be categorized into two methods, namely, pull-out tests and axial tension tests. The formulation of the bond-slip relationship has been developed for the following typical bond problems, as shown in Figure 14 [27]: (a) one side pull-out and (b) both sides pull-

out. In these tests, the main limitation is that they do not simulate the real conditions in a structural concrete member. Because of the effect of the compressive force (C), concrete is in compression and the reinforcing bar is in tension. The reality is different, in the tensile zone of a reinforced concrete member, the concrete and reinforcing bar are both in tension. The presence of a lateral stress modifies the stress distribution shown in Figures 14(a) and 14(b) to a considerable amount.

The distribution of tensile stresses induced in the reinforcing bar and concrete in the axial tests is be varied as shown in Figure 14(c). The difference opposed to pull-out tests resides in the absence of the compressive force C . This distribution is very similar to that of the tension face of a reinforced concrete flexural member in a three-point flexural test, which makes axial tests more suitable to simulate real-life conditions. [27]

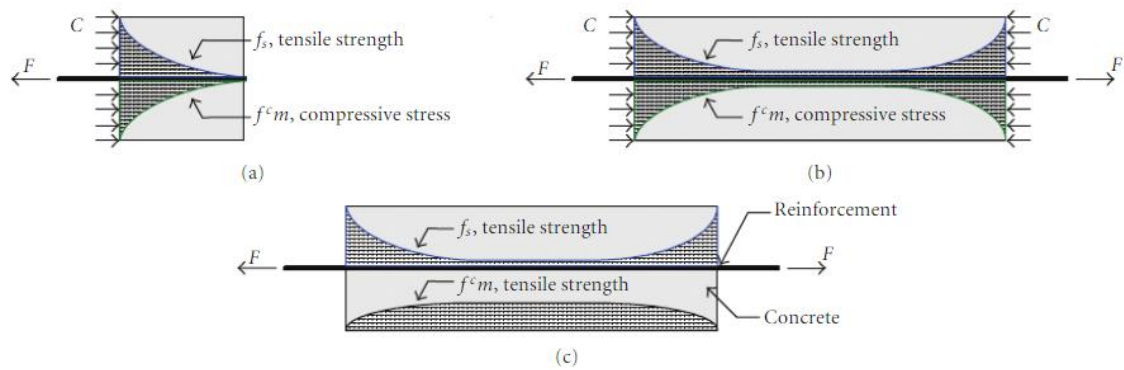


Fig. 14 Typical Stress Distributions for (a) One Side Pull-out, (b) Both Sides Pull-out, and (c) Axial Tension [27]

1.8.2 Irradiation device

The irradiating of the second part of the specimens prior to the bond testing will be done in the Universal gamma installation UGU – 420 in Minsk, Republic of Belarus, which can be seen in Fig. 15. [28] The State Scientific Institution «The Joint Institute for Power and Nuclear Research – Sosny» of the National Academy of Sciences of Belarus has been in the recent years actively developing radiation technologies, to include sterilization of medical devices and pharmaceuticals by means of electron and gamma-ray beams, modification of miscellaneous polymer materials, foodstuff treatment and other material experiments and could also serve for the experiment designed in this thesis [28]. Even though the BSC in nuclear reactors are subject to both neutron and gamma radiation, this experiment will only take into account gamma radiation, because neutron radiation tests are too expensive, demanding and dangerous.



Fig. 15 Universal Gamma Installation UGU – 420 [28]

The installation itself has a biological protection of water, a 1,5-meter-wide wall from reinforced concrete, and lead. There are two irradiation chambers, each with a volume of 33 m^3 . Irradiators itself are of length 100 cm, height 50 cm and distance 60 cm in between plates. The total number of sources is 768. Various geometry of irradiators is available, generating dose rate 0,1-10 Gy/s. The project capacity of the installation was $15,54 \cdot 10 \text{ Bq}$ (420 kCi), but as of September 2017 I was only $5,5 \cdot 10 \text{ Bq}$ (120 kCi).

The dose rate of a research nuclear reactor at the walls is about 200 Gy/h (0,055 Gy/s). [22] If we want to simulate a life cycle of a nuclear power plant, which lasts 40 years, the experiment would take approximately 20 years, if we presume the minimum dose rate of the installation – 0,1 Gy/s and 2 years if we calculate with the maximum – 10 Gy/s. A nuclear reactor with a prolonged license to 60 years could also be simulated, in this case in a 3 to 30-years-lasting experiment.

2 EXPERIMENTAL RESEARCH

2.1 Principle of the experiment

This experiment tries to determine the optimal method to measure the bond between biological shielding concrete and steel in reinforced concrete. The idea is, that irradiated and non-irradiated specimens will be submitted to testing of bond and the results will show how the bond is influenced by gamma radiation. In this part of the thesis the main goal is to find a setup suitable for experiments in an environment that works with irradiated samples, find an appropriate shape of the specimen and find out what is the desired character of failure. After design and testing we will have the first part of the data we need for comparison – the unirradiated specimen of concrete. The specifics of the second part of the experiment, the testing of irradiated samples, have been further discussed in the chapter 1.6 Proposal of the bond experiment in the Literature research part of this thesis.

2.2 Concrete mixture and design

The selected mixture is basically identical to that used in the NPPs operating in the Czech Republic. The same mixture has been used for experimenting with BSC in the past. However, the original mix design was adjusted, and coarse aggregate fractions were recalculated into the fine aggregate fractions to find the perfect grading curve. The reasons for this adjustment is the relatively small size of the specimens. For calculation of the content of each fraction, the Fuller formula was used.

$$y_F = \left(\frac{d_F}{D_{max}} \right)^{nF} \cdot 100 [\%]$$

where

y – percentage content of the calculated fraction [%]

D_{max} – maximum size of the grain [mm]

d – diameter of the grain [mm]

F – upper limit of the fraction [mm]

The prescription for one cubic meter is as follows in Tab. 3.

Part II: Experimental research

Tab. 3 Prescription of Concrete in Series 1

Quartz and serpentinite were used as the aggregate. Quartz as a representative of the most used aggregate for concrete in the Czech Republic and serpentinite as an example of a special aggregate used for biological shielding concretes. The serpentine has been chosen mainly because it is vastly used in NPPs for its high content of chemically bound water and the ability to retain it. Another reason is that it is a practical material due to its relatively low density of 2670 kg/m³. The samples were provided by a serpentinite quarry available in the Czech Republic. The properties of both aggregates can be seen in Tab. 4.

Tab. 4 Properties and Origin of Used Aggregates

Since series two no plasticizer has been used, content of water was adjusted accordingly, and the water ratio w/c changed. The content of water was enlarged by 5 %, ergo the water ratio raised to 0,401. This adjustment can be seen in Tab. 5.

Tab. 5 Prescription of Concrete in Series 2 and 3

2.3 Testing procedures

The specimen used for the testing needed to be of small dimensions so that a constant level of irradiation along the cross-section could be assumed. In larger specimens an exponential level would have to be assumed, as stated in the literature research. A cylinder has been chosen as an optimal shape for the experiment, because it is radially symmetrical, suitable for a circle rebar and the formwork is easily accessible.

The shape of the experimental surface has been defined as a cylinder of the height of 14,5 mm ($\pm 0,5$ mm), the radius of 42 mm with a smooth steel rebar in the middle with the radius of 9 mm. As formwork, petri dishes were used.

To achieve a one hundred percent repeatable test, no plasticizer has been used (since series two). All the experiments were controlled by displacement. The specimens were tested after 28 days since production, during this time they were covered with a foil to achieve 100 % humidity curing. A scheme of the specimen with dimensions can be seen in Fig. 16.

Part II: Experimental research



Fig. 16 Dimensions of the Specimen

In order avoid local pressures and assure the repeatability a rebar with a smooth surface has been used. An ideal form of a bond test is a perfect shear-only test with no other forces in the concrete than shear forces. This test included pushing the rebar through rather than pulling it out, because it is technologically easier. The scheme of the test can be seen in Fig. 17.



Fig. 17 Scheme of the Test

The force was applied by a second smaller rebar (the radius of 8 mm) and the supports were created by a metal pipe supporting the specimen in the geometrical center, both were considered to be infinitely stiff. The machine moved at a constant rate of 1 or 2 millimeters per minute and the applied force was measured.

Three series of tests have been executed. The first two series included three concrete specimens each with a steel rebar and quartz aggregate. The third series counted

Part II: Experimental research

six quartz and six serpentinite specimens. Due to the size of the cylinder it was not an option to reinforce it with for example thin metal wires.

2.3.1 Series 1

In order to avoid unnecessary bending moments, two metal sheets were installed around the tested specimen, one of which was supposed to serve as another line supports, see Fig. 18 and 19.



Fig. 18 Additional Reinforcement in the First Series of Tests

The tension in the rebar is much smaller than the strength of the steel (S235JR) and therefore it is considered to be infinitely stiff. However, the metal sheets were not stiff enough to create the necessary supports and the first series of testing resulted in the classic one-point bending test and the concrete broke into three pieces, see Fig. 20.



Fig. 19 Assumed Reduction of Internal Forces, First Series of Tests



Fig. 20 Damage to the Specimen in the First Series of Tests

The dependence of applied force and translation can be seen on Fig. 21. Each specimen shows the trend of two peaks. The first is the infraction (for specimens no. 2 and 3 gradual) of the concrete from bending moments, the second reaching the maximum

Part II: Experimental research

bond stress. The loading rate of the test was 2 mm/min and the maximum applied force was 3,18 kN. Quartz was used as an aggregate.

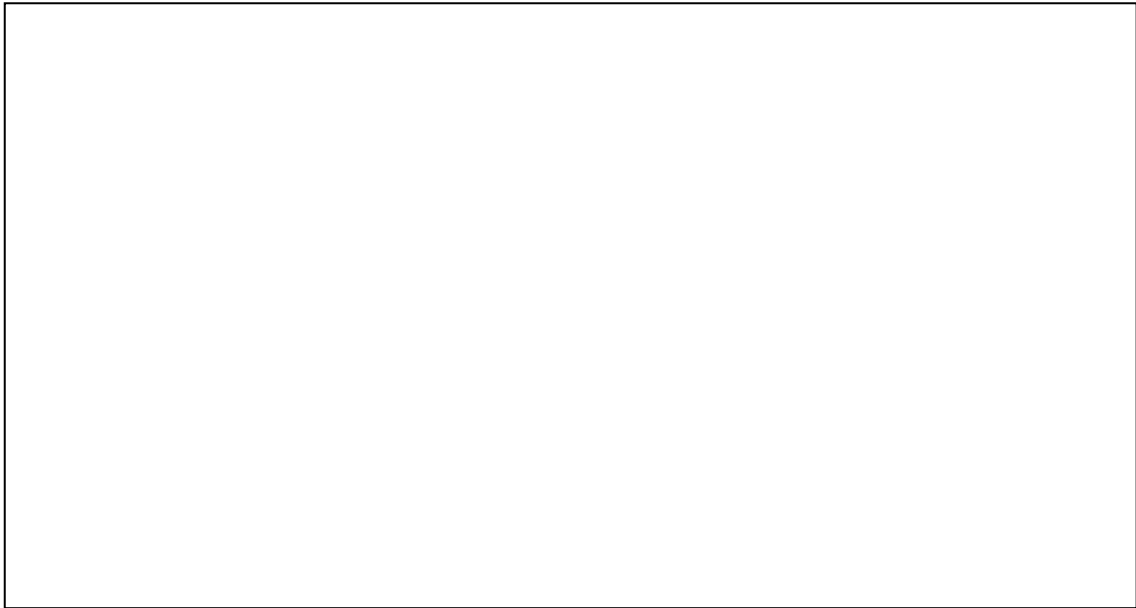


Fig. 21 Dependence of Applied Force and Displacement in the First Series of Tests

2.3.2 Series 2

The second series of tests was done on same specimens, but a smaller metal pipe was used, again to avoid bending moments. If the supports were installed too close to the interface of steel and concrete, the concrete would be crushed near the supports. Therefore, a minimum distance of two millimeters was maintained. Quartz was used as an aggregate.

Certain bending moment has been noted and a crack appeared on the surface of all three specimens, always in the direction of the maximal eccentricity. However, after the initial appearance of the crack and the fall of the affecting force (reaching the maximum bond stress), the dependence of force and displacement created a nearly straight line and the angle can be clearly observed. The crack is not visible in the graph.

The average maximum bond stress of the three specimens was 6,12 MPa, the maximum applied force was 5,05 kN. The specimen stayed intact as can be seen in Fig. 22.

Part II: Experimental research

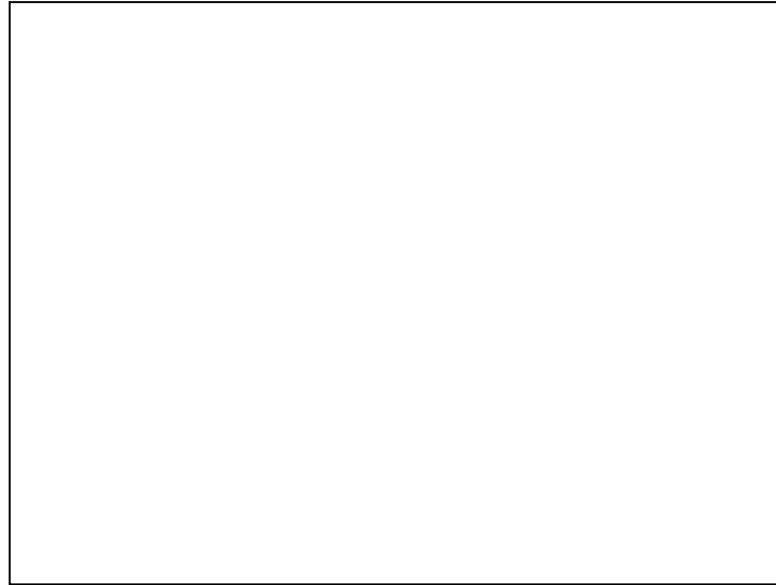


Fig. 22 The Intact Specimen in the Second Series of Tests

The graph of the loading of the second series of tests can be seen in Fig. 23. The loading rate of the testing was 1 mm/min. The graph corresponds with the schematic bond-slip relationship, a splitting failure [7]. A small imperfection in the flow of the dependence in case of Specimen 2 was caused by small bumps on the rebar. This can be seen in Fig. 24.



Fig. 23 Dependence of Applied Force and Displacement in the Second Series of Tests

Part II: Experimental research



Fig. 24 The Imperfections Present in Specimen 2 in the Second Series of Tests

Fig. 25 shows the bond stress in the second series of tests. At the beginning the maximum bond stress is reached, at the end the stress rises because only a small contact area remains effective. The rise of the stress can also be influenced by possible jamming of the rebar in the concrete.



Fig. 25 Dependence of Bond Stress and Displacement in the Second Series of Tests

In the middle part of the diagram, the stress is approximately constant and is defined by material properties. This part of the diagram is considered to be the valid range.

The constant level proves that the interface is the same along the cross section. This part of the diagram is called valid range, because the premise of a constant bond stress is met.

2.3.3 Series 3

In order to confirm the results of the successful second series, a third series was performed in the same way as the second series, meaning that the loading rate of the test was 1 mm/min and the way of loading remained the same. Twelve specimens have been created. In specimens K1 – K6 quartz has been used as an aggregate, in specimens S1 – S6 serpentinite has been used. Comparison of specimens of the third series can be seen in Fig. 26.

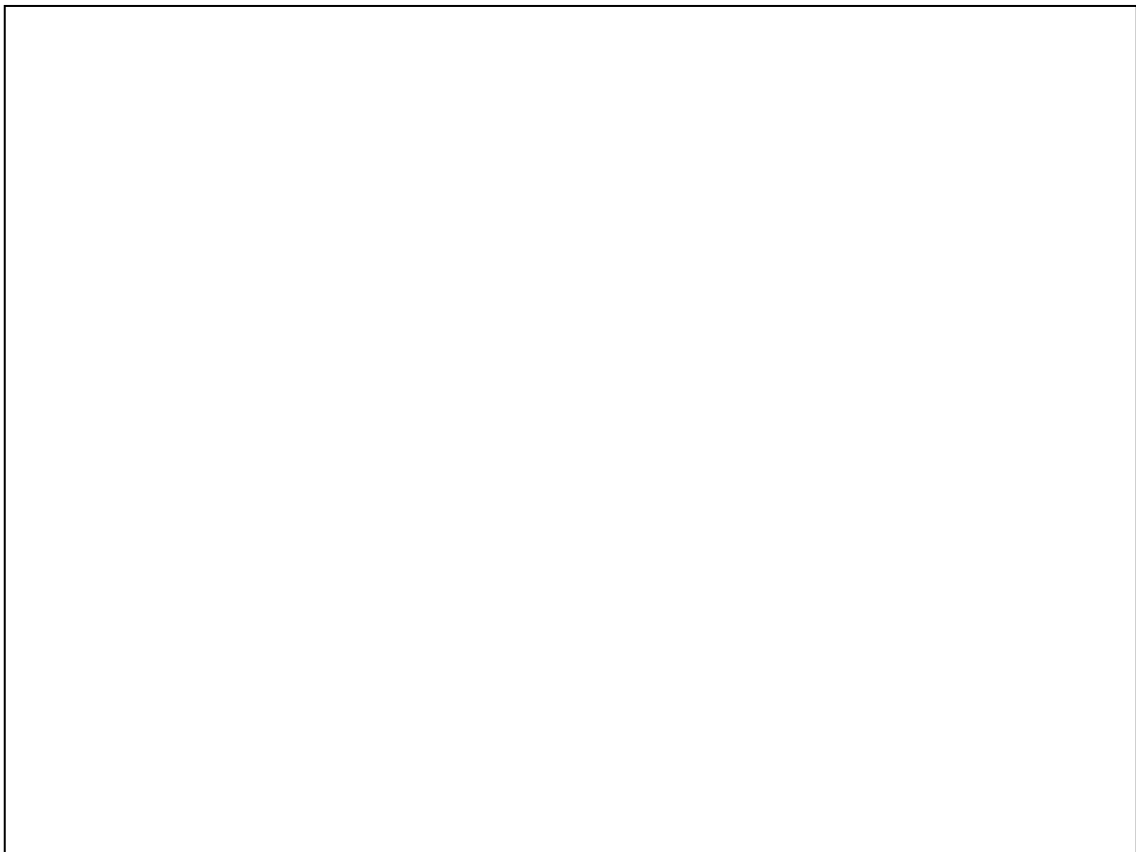


Fig. 26 Specimens of the Third Series of Tests – S-Serpentinite Aggregate, K-Quartz Aggregate

In this picture we can see that during the 28 days of concrete strengthening rust has already begun to damage the specimen at the cross-section. This is can probably be adjudged to the 100 % humidity caring of the samples. In future this issue could be taking into consideration, for example by treating the surfaces with a substance or coating, because the future experiments including irradiation will take much longer than 28 days and the progressing rust could influence the quality of the steel-concrete bonding area.

Part II: Experimental research

The maximum applied force was 3,51 kN in case of quartz (specimen K3) and 3,31 kN in case of serpentinite (specimen S5). The average maximum bond stress of the six quartz specimens was 4,096 MPa, in case of serpentinite the average maximum bond stress of the six specimens was 3,806 MPa. Quartz aggregate reached higher results of forces and stresses than serpentinite aggregate, but the difference was not so significant. The graph of the loading of the third series of tests can be seen in Fig. 27.

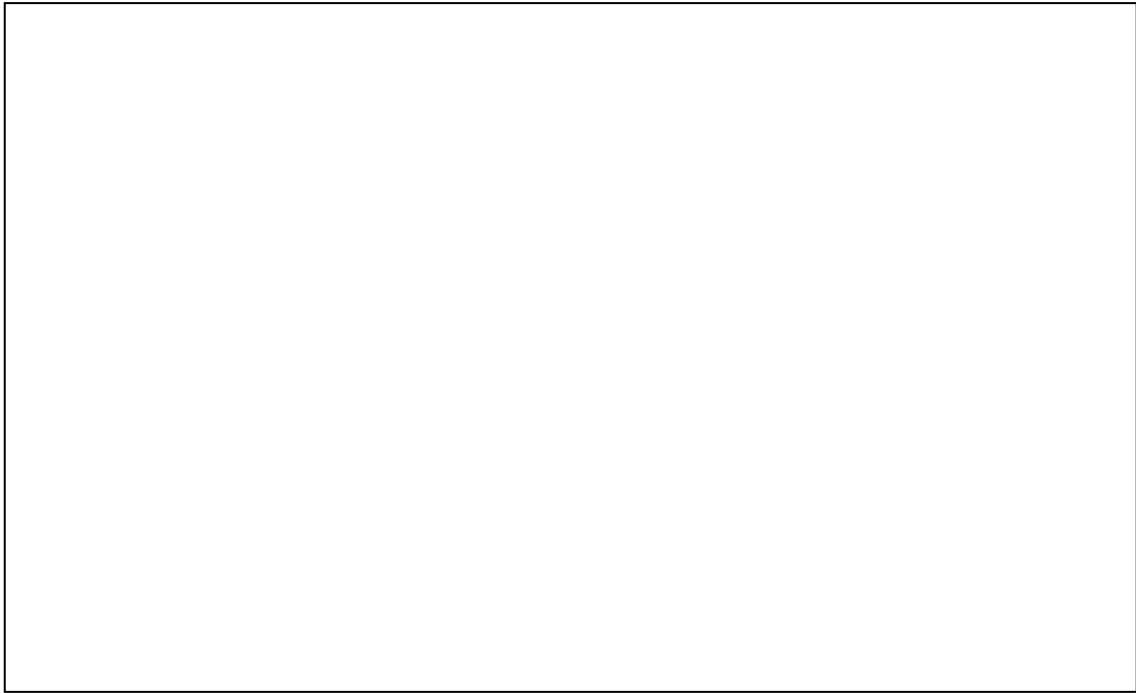


Fig. 27 Dependence of Applied Force and Displacement in the Third Series of Tests

In Fig. 27 it can be seen that nine of all the specimens have suffered a different character of failure than the one which was observed in the second series and three specimens (S2, K1 and K6) followed its path, the first character of failure. Unlike the first character of failure there is no great fall in values of applied force in case of the second character of failure, the force is only linearly getting smaller. No correlation was observed between these two groups and no reason was found for this particular behavior. These results tell us that the second character of failure occurred more times than the first character (nine times in series two versus three times in series two and three).

Generally, the flow of the diagram is suitable for a bond test, the bond coefficient is linear, a straight line can be fitted. The valid range represents the linear part of the diagram. Fig. 28 shows the bond stress in the second series of tests.

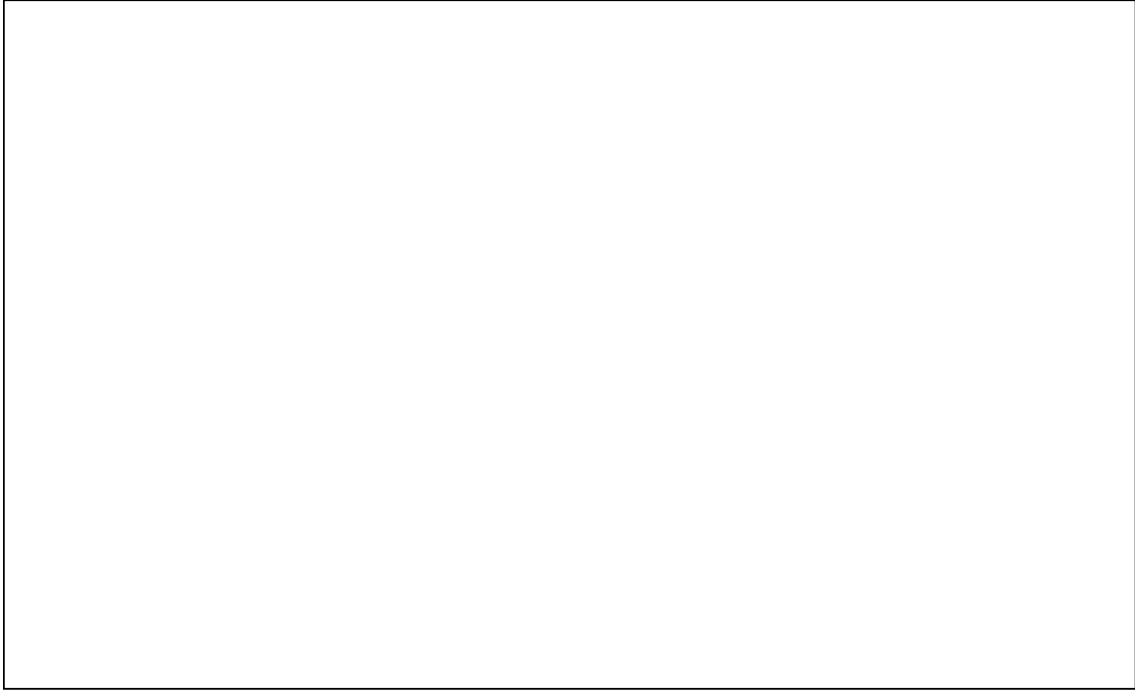


Fig. 28 Dependence of Bond Stress and Displacement in the Third Series of Tests

The graph in Fig. 28 corresponds with the results of bond stress in the second series of tests. All values of bond stress rise out of limits toward the end of the diagram except for specimen S5. This was probably caused by severe damage to the bond layer of the concrete-steel interface. The valid region can again be seen as the middle part of the diagram where the stress is close to a constant.

The overall results are summarized in Tab. 7. The results of the first series are almost as high as the results of the following series, but these values of maximum stresses have been measured during an atypical and unwanted kind of character of failure. Interesting noted behavior is that even though only the first series included plasticizer (since second series it was left out because of repeatability), it shows lower values of force and bond stress than the second series.

The values of maximum bond stress do not include the extreme values in the end of loading, which are caused by a small remaining bonding area.

Part II: Experimental research

Tab. 7 Results of Series 1, 2 and 3 – Maximum Applied Forces and Maximum Bond Stresses

3 NUMERICAL MODELLING

3.1 Objective

The objective of the numerical modelling part of the thesis was to program a non-linear model using the finite element method, which would correspond with the data obtained in the experimental part of the thesis. As a development environment, MATLAB was chosen for its vast number of integrated libraries and functions and its orientation on programming of engineering problems.

3.2 Axisymmetric elements

The finite elements used were special two-dimensional elements called the axisymmetric elements. Due to the use of axisymmetric elements, a 3D problem was reduced to a 2D problem. This type of element is useful in case of symmetry about an axis of the body being analyzed, given that the symmetry respects the geometry and loading. Axisymmetric elements are used to analyze circular objects such as pressure vessels. In Fig. 29 [29], an axisymmetric problem of a circular structure can be seen, which can be solved using the axisymmetric elements. In Fig. 29, we can also notice that the three-dimensional body is reduced to a two-dimensional section thanks to the symmetry about the central axis.

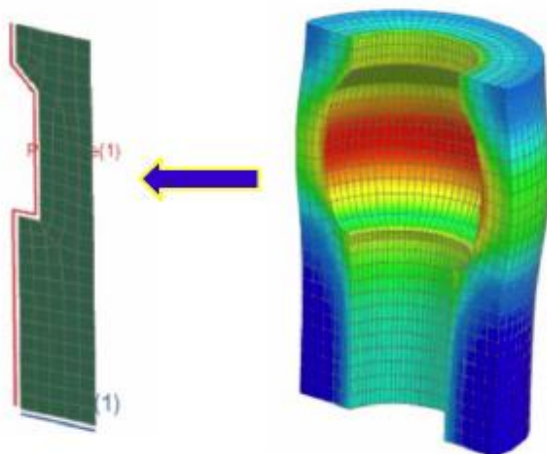


Fig. 29 Axisymmetric Problem of a Circular Structure Reduced to a Section and the Corresponding Finite Element Mesh [29]

In Fig. 30 [29] an example of a triangular torus with the principal axes r and z can be seen. All triangular axisymmetric elements, which is the shape used in this thesis, are in fact triangular tori symmetric about the z axis. The z axis is called the axis of symmetry, each vertical cross-section of the triangular torus is a triangle. The circumferential coordinate is labeled θ , principal coordinates r and z coincide with the principal axes r and z [29].

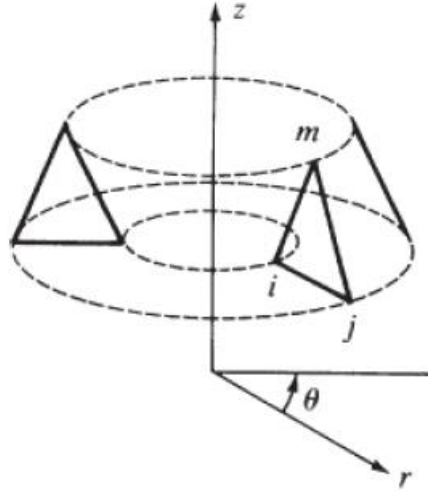


Fig. 30 *Triangular Torus with Principal Axes r and z and the Circumferential θ Coordinate [29]*

The planar axisymmetric formulation of an object is similar to planar stress/strain formulation, but often not considered as a separate category. It is actually equivalent to the plane strain formulation in cylindrical coordinates and all properties of plane strain elements are equivalent to axisymmetric elements. Plane strain elements assume that the object is so thick, that the strain components in the main direction are zero. Unlike the plain strain elements which are calculated by a 3×3 constitutive matrix and a 3×1 stress/strain vector, the axisymmetric formulation produces a 4×4 constitutive matrix and a 4×1 stress/strain vector [30]. The isotropic stress-strain relationship, obtained by simplifying the general stress-strain relationships is:

$$\begin{Bmatrix} \sigma_r \\ \sigma_z \\ \sigma_\theta \\ \tau_{rz} \end{Bmatrix} = \frac{E}{(1+\nu)(1-2\nu)} \begin{bmatrix} 1-\nu & \nu & 0 & 0 \\ \nu & 1-\nu & 0 & 0 \\ 0 & 0 & 1-\nu & 0 \\ 0 & 0 & 0 & 0.5-\nu \end{bmatrix} \begin{Bmatrix} \varepsilon_r \\ \varepsilon_z \\ \varepsilon_\theta \\ \gamma_{rz} \end{Bmatrix}$$

where

$\sigma_r, \sigma_z, \sigma_\theta, \tau_{rz}$ – normal and tangential stresses in direction of principal coordinates [Pa]

Part III: Numerical modelling

$\varepsilon_r, \varepsilon_z, \varepsilon_\theta, \gamma_{rz}$ – relative strains in direction of principal coordinates [m/m]

E – modulus of elasticity [Pa]

ν – Poisson's ratio [-]

3.3 Derivation of the stiffness matrix

The axisymmetric solid was discretized by typical triangular elements. The element displacement functions were considered linear triangular shape functions. From this the strain-displacement and stress-strain relationships mentioned above could be derived. The stiffness matrix can be defined as:

$$[K] = \int_V [B]^T [D] [B] dV$$

where

$[K]$ – stiffness matrix of an axisymmetric element [N/m]

For a circumferential differential element, the integral becomes:

$$[K] = 2\pi \int_A [B]^T [D] [B] r dr dz$$

where $[B]$ matrix is a function of r and z

$[K]$ matrix is therefore a function of r and z and is of order 6 x 6. It can be evaluated by one of three methods:

1. Numerical integration (Gaussian quadrature)
2. Explicit multiplication and term-by-term integration
3. Evaluate $[B]$ for a centroidal point with coordinates r^C, z^C , which are the average coordinates of the three coordinates of triangle corners. If the triangular subdivisions are consistent with the final stress distribution (that is, small elements in regions of high stress gradients), then acceptable results can be obtained by method no. 3. The approximation results in:

$$[B(r^C, z^C)] = [B^C]$$

$$[K] = 2\pi r^C A [B^C]^T [D] [B^C]$$

3.4 Application of the axisymmetric elements

The triangular mesh of the problem can be seen in Fig. 31. It is a half of a symmetrical cross-section of a solid body represented in the experimental part of this thesis – a cylinder of radius 42 mm and height 14,5 mm with a steel rebar in the middle of radius 9 mm. The dimensions were adjusted to even numbers to achieve a regular mesh, where all triangles are equally big. The area of all triangles was 10^{-6} m^2 .

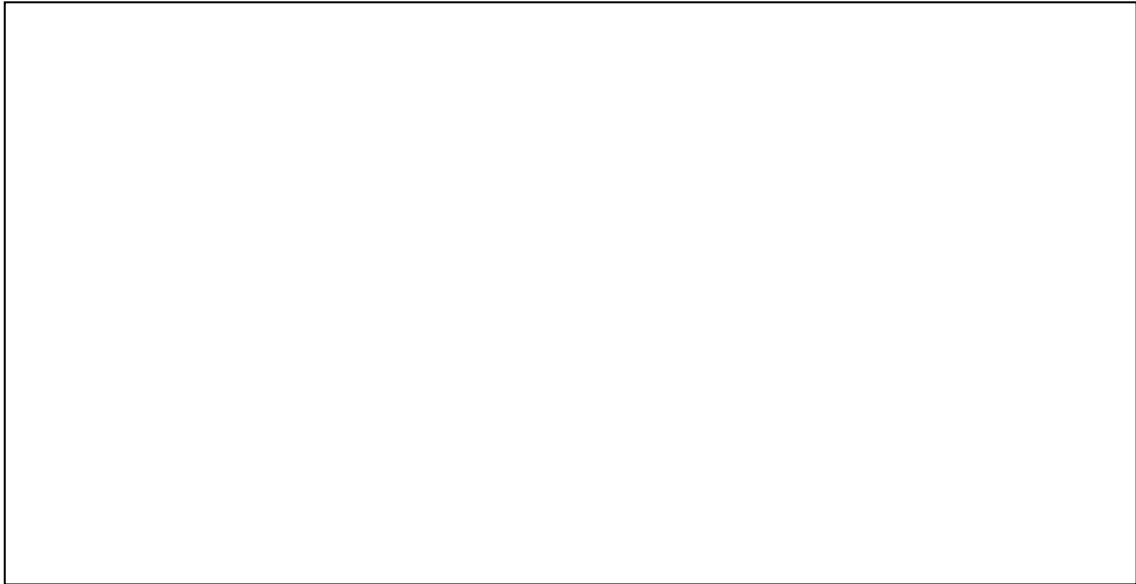


Fig. 31 Triangular Mesh of the Problem with Supports and Loading

Local stiffness matrices were localized into a global stiffness in a usual matter. The resulting global matrix was sparse, the dimensions were 704 x 704. The global matrix was evaluated by method no. 3 mentioned in the previous chapter for its simplicity and because it can be effectively programmed [29].

In Fig. 31 boundary conditions and character of loading can also be seen. The supports on the lower edge of the mesh are modelled according to the experimental part of the thesis while the purpose of the other supports, which prevent only one degree of freedom, is modelling the symmetry. This approach is called the condition of symmetry and the advantage is that only half of the specimen needs to be modelled.

3.5 Method of modelling the bond layer

Two different methods of modelling the bond layers were used, the description of each is written below.

3.5.1 Lagrange multiplier method – multi-point constraints

The method of Lagrange multipliers (or multi-point constraints) is a mathematical strategy for finding the local maxima and minima of a function subject to the condition that certain equations have to be satisfied exactly by the chosen values of the variables. In the FEM, the multi-point constraints are used for modelling of joints, for example to connect a turbine blade with a turbine disc. Another example would be to join a column and a 2D solid accompanied by minimizing the number of DOFs – preventing the rotation of the column and extending the column into the 2D solid.

In a case of the bond layer problem the multi-point constraint can be used to tie together the displacements of the nodes in the bond layer, which are depicted in Fig. 32.

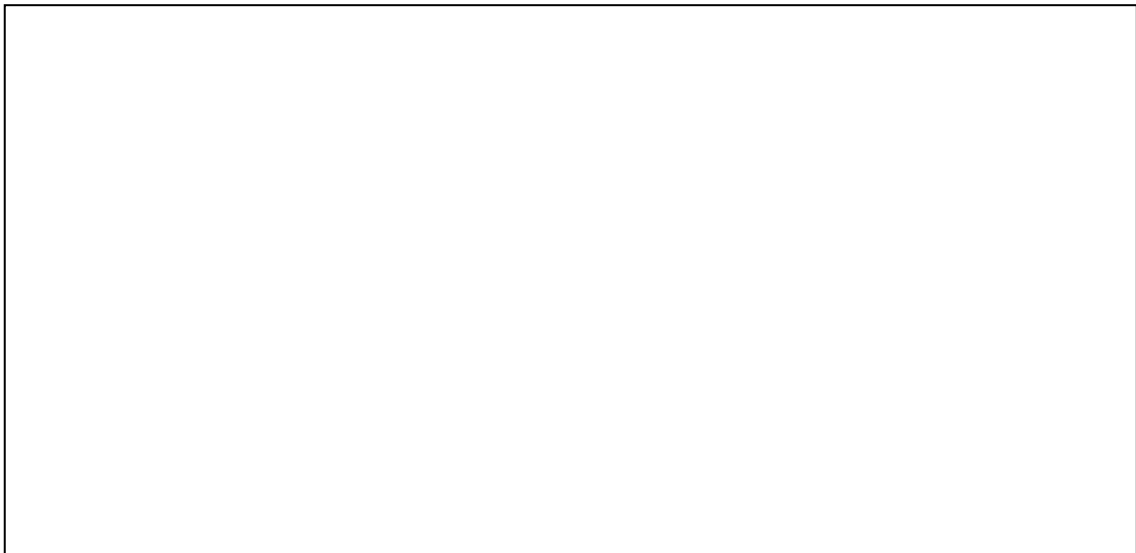


Fig. 32 Triangular Mesh of the Problem with Multi-point Constraints in the Bond Layer

The stiffness matrices of the concrete and steel section were created separately and assembled along with the constraints, as can be seen in the scheme in Fig. 33 [31], which is called the bordered stiffness. The MPC are appended as additional equations and the whole system is called the multiplier-augmented system. For each of the constraints, in this particular case sixteen were needed as can be seen in Fig. 31, the global matrix gets bigger by one row and one column. This extra row or column makes the same bond displacements figured in both the concrete and steel matrices equal. The vector of unknowns grows by the value alpha, which is the force needed to ensure the functioning of the constraint. The load vector contains a new value, a number which represents the distance of the two constrained nodes, in this case zero. [31]

$$\begin{bmatrix}
 K_{11} & K_{12} & 0 & 0 & 0 & 0 & 0 & 0 \\
 K_{12} & K_{22} & K_{23} & 0 & 0 & 0 & 0 & 1 \\
 0 & K_{23} & K_{33} & K_{34} & 0 & 0 & 0 & 0 \\
 0 & 0 & K_{34} & K_{44} & K_{45} & 0 & 0 & 0 \\
 0 & 0 & 0 & K_{45} & K_{55} & K_{56} & 0 & 0 \\
 0 & 0 & 0 & 0 & K_{56} & K_{66} & K_{67} & -1 \\
 0 & 0 & 0 & 0 & 0 & K_{67} & K_{77} & 0 \\
 0 & 1 & 0 & 0 & 0 & -1 & 0 & 0
 \end{bmatrix}
 \begin{bmatrix}
 u_1 \\
 u_2 \\
 u_3 \\
 u_4 \\
 u_5 \\
 u_6 \\
 u_7 \\
 \lambda
 \end{bmatrix}
 =
 \begin{bmatrix}
 f_1 \\
 f_2 \\
 f_3 \\
 f_4 \\
 f_5 \\
 f_6 \\
 f_7 \\
 0
 \end{bmatrix}$$

concrete steel

Fig. 33 Scheme of the Lagrange Multiplier Method [31]

After deploying this method, the resultant global stiffness matrix was singular, the rank of the matrix was 570 instead of wanted 695 and the system could not be calculated. Therefore, a second method of modelling the bond layer was used, which is described in the next chapter.

3.5.2 Differentiation of stiffness in the bond layer

The approach of the second method is to differentiate the diverse parts of the model according to reality including the bond layer. The modulus of elasticity of concrete and steel was set to known values. The modulus of elasticity of the layer of finite elements in the bond layer (which can be seen in Fig. 31) was set to a much smaller value to achieve the same character of failure as in the experimental part and then later iterated to fit the model and stress-strain relationship to the experiment. This approach was combined with the nonlinear Modified Newton-Raphson method with the goal of a non-linearly behaving bond layer, this method is introduced in the next chapter.

3.6 Nonlinear static analysis

Linear static analysis presumes that the relationship between loads and the induced response is linear. We must use the nonlinear analysis if one or more of these linearity assumptions fail:

1. All materials in the model comply with Hook's law, meaning that stress is directly proportional to strain. This is usually valid only in case of small strains. Nonlinear analysis offers a lot of different types of models.

2. The displacements are so small that the change in stiffness caused by loading can be ignored. In nonlinear analysis, the stiffness matrix can be recalculated at every solution step.
3. Boundary conditions do not vary during the loading. Loads must be constant, they should not change while the model is deforming. Contact problems are naturally nonlinear because the boundary conditions change upon loading, linear analysis can only approximate the solution when the large deformation effect is considered.

Nonlinearities are divided between geometric, material and contact. There are different numerical procedures that can be used in the solution of nonlinear problems in the FEM. It always contains a control technique, capable of controlling the progress, an iterative method and termination schemes to end the solution process. [32]

3.6.1 Incremental control techniques

Various control techniques have been used to perform nonlinear analysis. These techniques can be divided into [32]:

1. Incremental load control method

This strategy uses loads applied to the system as prescribed variables. Each state of the equilibrium is found as the intersection of the constant incremented load (a surface) and the corresponding displacements. One value of force can correspond to two different values of displacement.

2. Incremental displacement control method

In this method a specified degree of freedom is controlled. It is incremented by using a ‘time curve’. The pattern of the applied loads is incremented proportionally to the displacement of the controlled DOF. The advantage of the displacement-controlled procedure in comparison to the force-controlled (or load-controlled) is that the first one can be more stable than the latter one, as can be seen in Fig. 34 [33]. It is easier to reach point D, where the load starts reducing, which the force-controlled method finds with difficulties because the system reaches equilibrium at point B with the given load F_B . Another advantage of this method lies in the fact that the behavior of the system is unknown in advance. Therefore, if a load greater than F_C is applied, the iteration will not converge and no solution exists. The displacement-controlled procedure can converge the

solution in a broader range of displacements. Each value of displacement corresponds with only one value of the force. [33]

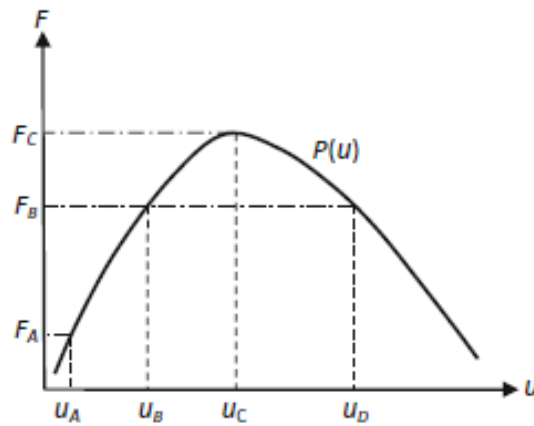


Fig. 34 Example of the Incremental Displacement Control Method [33]

3. Incremental arc-length control method

Unlike former methods, where one of the axes is used to control the analysis, here a special parameter is prescribed by means of a constraint, which is added to the set of equations governing the system equilibrium. When geometrically speaking, the parameter can be imagined as the ‘arc length’ of the resultant path. All three control techniques are depicted in Fig. 35 [32].

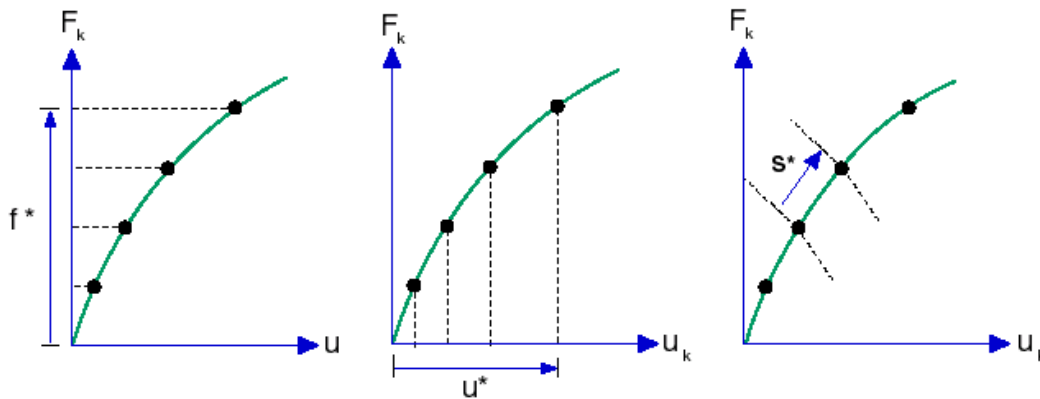


Fig. 35 Incremental Control Techniques – Load Control (on the left), Displacement Control (in the middle) and Arc-Length Control (on the right) [32]

3.6.2 Iterative solution methods

In nonlinear statics, the basic equation to be solved at every step, $t+\Delta t$, is:

$$R^{t+\Delta t} - F^{t+\Delta t} = 0$$

where

$R^{t+\Delta t}$ – vector of externally applied nodal loads [N]

$F^{t+\Delta t}$ – vector of internally generated nodal forces [N]

The internal nodal forces depend on nodal displacements at time $U^{t+\Delta t}$, therefore an iterative method must be used. Different schemes of iterations exist, most important ones are described further [32]:

1. Newton-Raphson Scheme

In numerical modelling, the Newton-Raphson method is used to find better approximations to the roots of functions. In the diagram in Fig. 36 [32] it can be seen, that the tangential stiffness matrix is formed and decomposed in every iteration in every step. Recalculating the stiffness matrix can be truly expensive for complex models. However, the NR method has a quadratic rate of convergence, the rate of convergence is high.

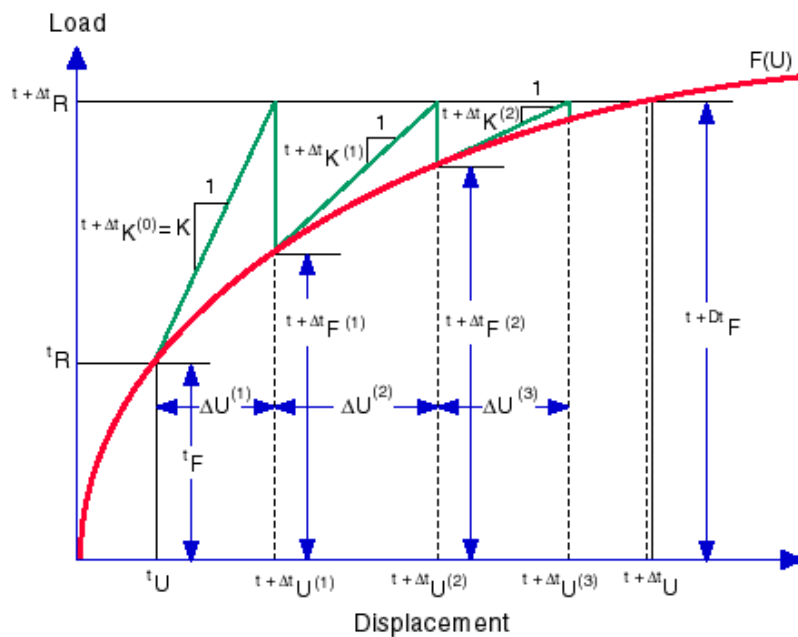


Fig. 36 Iterative Solution Methods – Diagram of One Step in the NR Method Scheme [32]

2. Modified Newton-Raphson Scheme

When the NR scheme cannot be used because of computation time, MNR can serve well. In this case, the tangential stiffness is the same for all the iterations in one step as shown in Fig. 37 [32] below. The matrix can be formed and decomposed at the beginning of each step or stay the same for all of the steps, as specified when defining the

properties of the analysis. From comparison of both diagrams the MNR is slower to get to the result, but easier to apply.

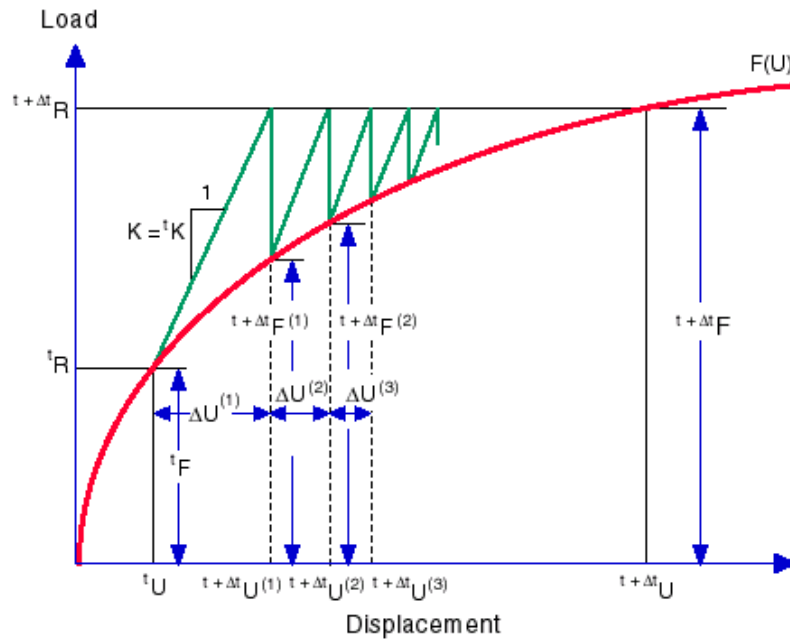


Fig. 37 Iterative Solution Methods – Diagram of One Step in the MNR Method Scheme [32]

3.7 Application of the nonlinear static analysis

In this numerical modelling part of the thesis, nonlinear static analysis was used. The concrete and steel elements were analyzed linearly, the bond elements nonlinearly. The premise of linearity of concrete elements was validated by the fact that the stress in concrete elements was in the linear part of the stress-strain diagram of concrete. The incremental control technique was an incremental displacement control method, which is exactly in compliance with the experimental part of the thesis, the experiment was also displacement-controlled.

Fifteen steps were executed, each moving the top layer of the steel 1 mm downwards, so at the end the two parts of the model are detached. An outer for loop iterated these fifteen steps, an inner while loop iterated the iterative MNR method. In the outer loop, nonlinear stresses and local internal forces were calculated. A global matrix of forces was calculated. In the inner loop, differential displacements were calculated from the stiffness matrix and the global forces, displacements were added to initial displacements and the while loop ran until the global forces were in tolerance (set to 0,000001), the displacements did not increase anymore, which means the solution was

found. Total displacements in directions of axes r and z are depicted in Fig. 38 obtained from MATLAB. In the picture, it can be clearly seen, that the concrete and steel parts behaved linearly while the layer of the bond elements was completely destroyed.

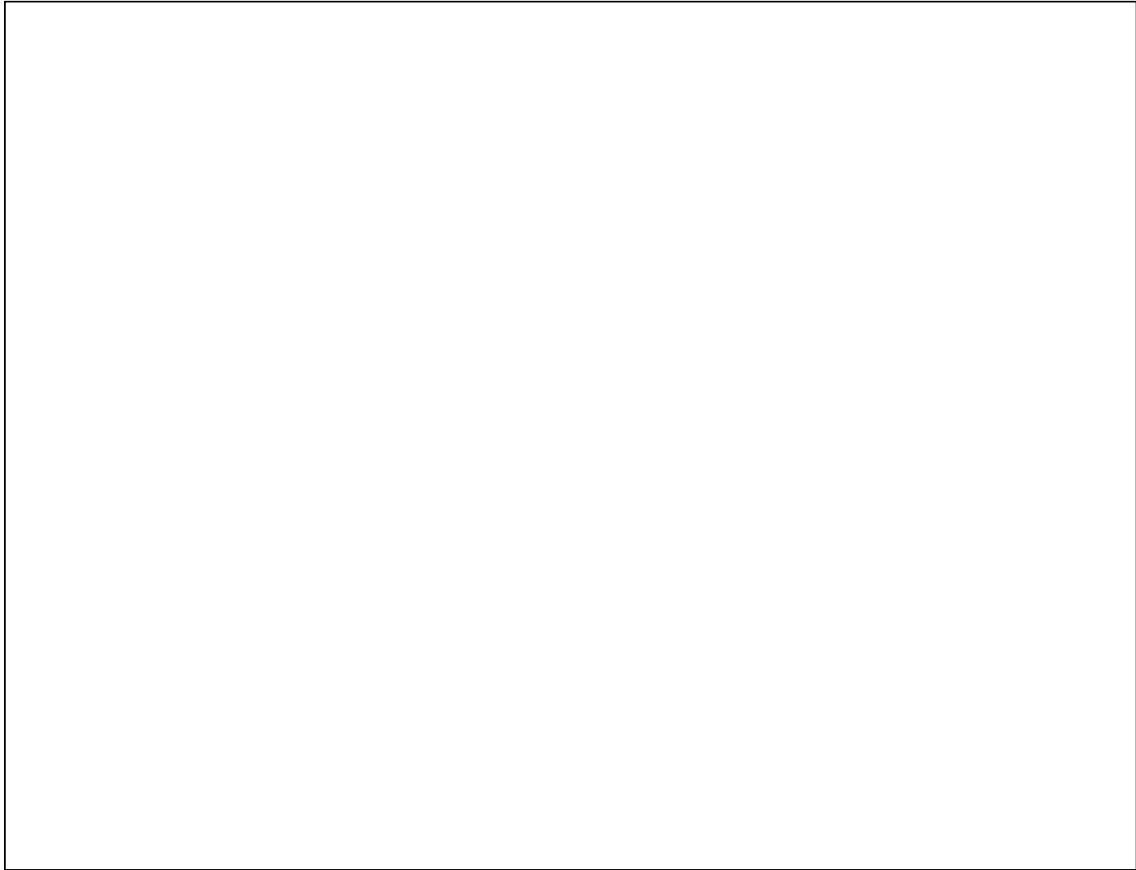


Fig. 38 Total Displacements in Directions of Axes r and z

Since there were two different characters of failure, two types of dependences of applied force and displacement in the third series of tests (Fig. 27), two different charts were found to fit them. The size of the two vertical reactions in the bottom of the model, which can be seen in Fig. 31, was plotted over the fifteen steps and fitted to the two different characters of failure. The size of the reactions is equal to the theoretical applied force to the model, which is the result of MNR. The chart of vertical reactions from MATLAB can be seen in Fig. 39 and a comparison to the experimental part of the thesis in Fig. 40.

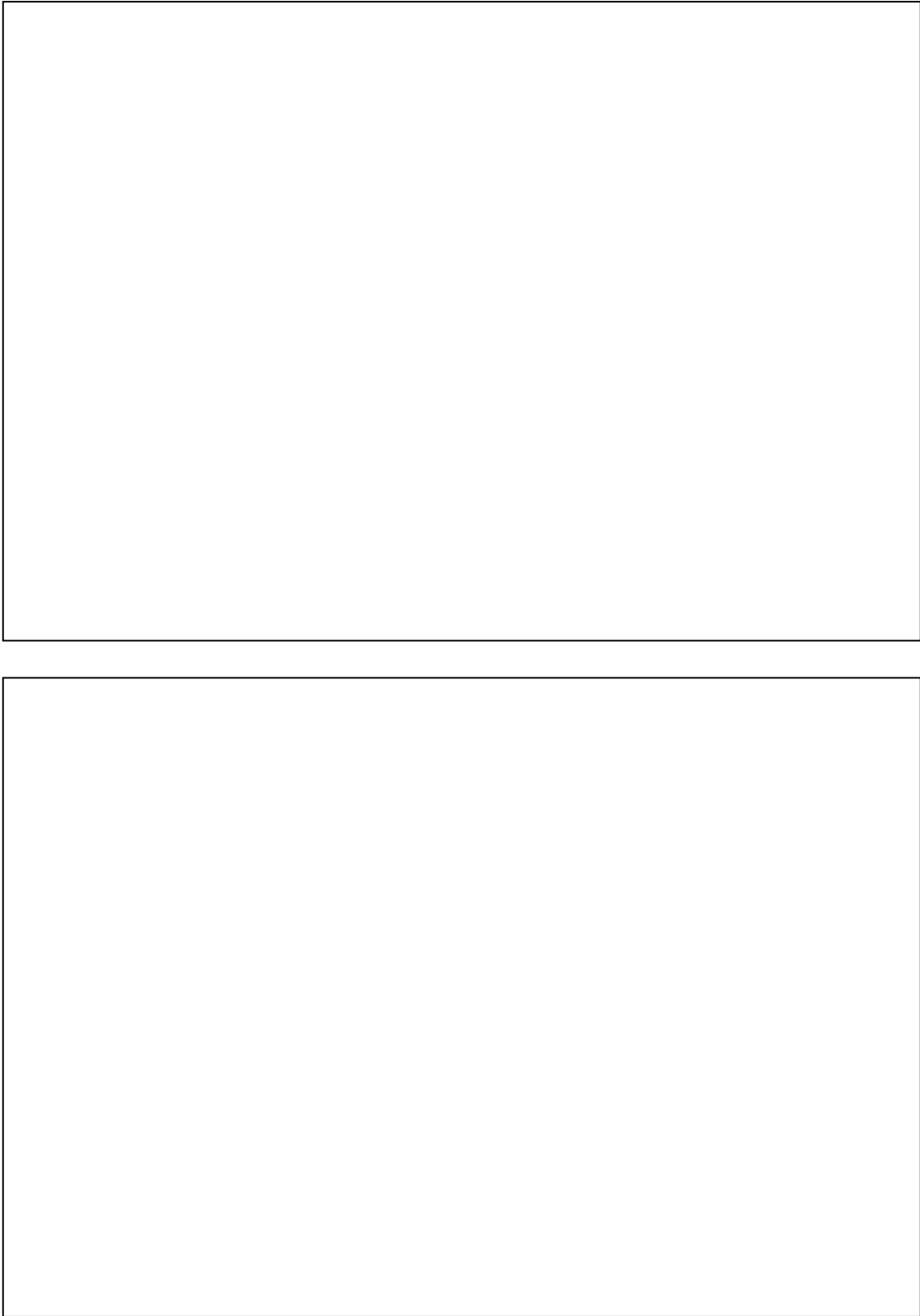


Fig. 39 Dependences of Applied Force and Displacement from MATLAB Corresponding to the First Character of Failure (upper) and the Second Character of Failure (lower)

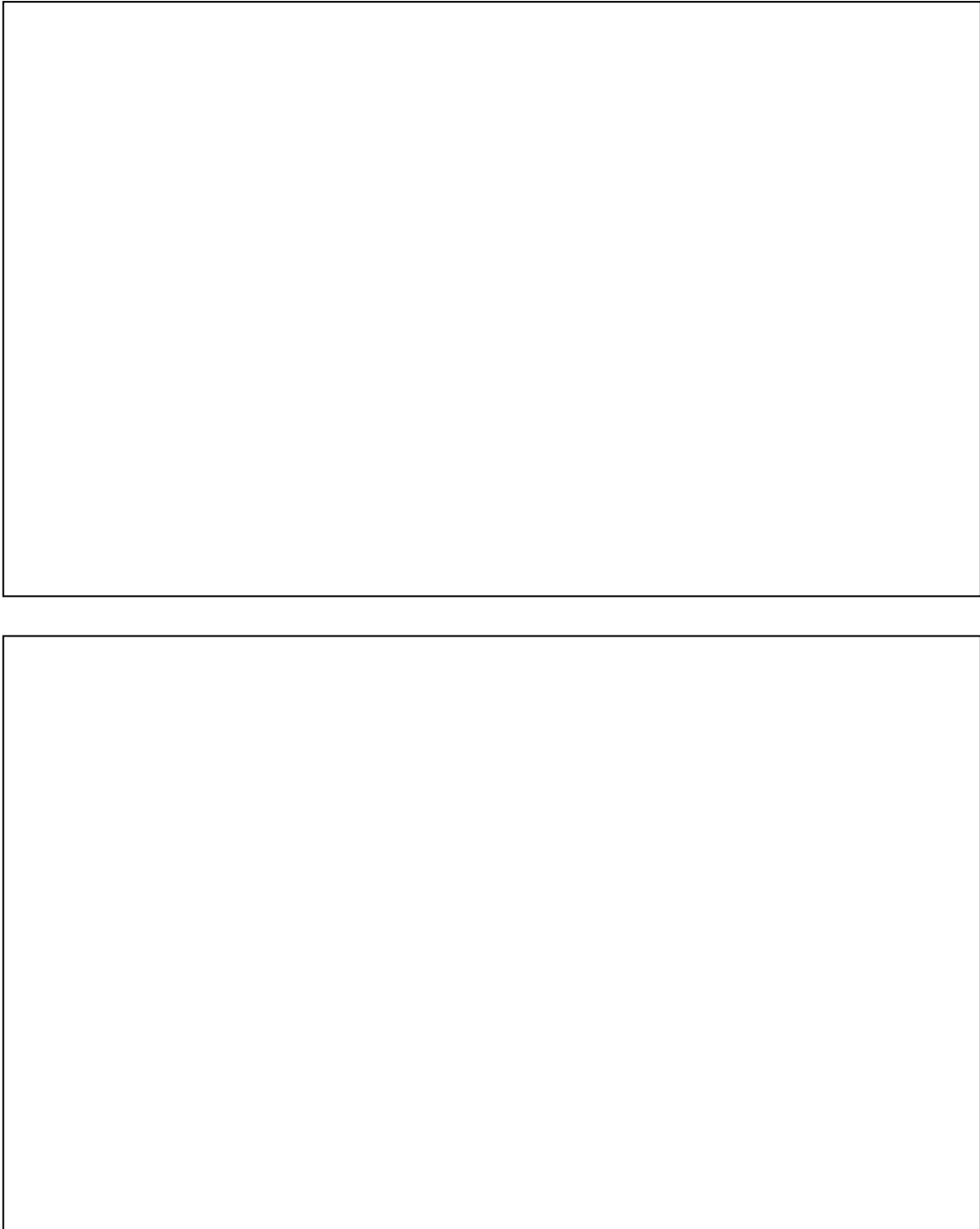


Fig. 40 Comparison of Dependences of Applied Force and Displacement from MATLAB and the Experiment Fitted to the First Character of Failure (upper) and the Second Character of Failure (lower)

The charts of applied forces are limited to a small part of the diagram beyond the ultimate strength. The reason is that this model cannot capture the slip part of the experiment, a contact model, e.g. the Bingham model, would be a solution to display the rest of the diagram.

Part III: Numerical modelling

To the input parameters belongs a stress-strain diagram of the bond elements depicting the ultimate strength in compression and tension. This diagram was iterated to fit the numerical model to the experiment.

Two parameters have differed for the two characters of failure – firstly the stress-strain diagram and the modulus of elasticity of the bond elements. The stress-strain diagrams for both cases can be seen in Fig. 41.

In the first case the modulus had a value of 4 GPa, in the second case 7 GPa. The modulus of elasticity of concrete was assumed 25 GPa, for steel 210 GPa. The maximum linear strain in the stress-strain diagram was set to 0,001 for both cases.

Poisson's ratio was set to 0,3 for steel, 0,2 for concrete and 0,1 for the bond elements as an interpolation between the value for concrete and the value for air, which is zero.

Bond damage coefficient was established. If the specific bond element acted nonlinearly, which was true to all of them, the γ_{rz} part of the stress vector was lessened and calculated according to the input stress-strain diagram. γ_{rz} was always the largest value of the stress vector in the bond element, since the strain was mostly tangential. The damage coefficient of the bond elements was defined as:

$$D = \frac{E_{new}}{E_{old}}$$

where

D – the damage coefficient [-]

E_{new} – modified modulus of elasticity [Pa]

E_{old} – original modulus of elasticity [Pa]

This damage coefficient was used to modify all other parts of the stress vector, meaning σ_r , σ_z , σ_θ to ensure a damage model behaving according to reality – isotropic damage. Instead of the damage coefficient, a deviator could be used in real-life structures, which would determine the prevailing part of the stress vector.



Fig. 41 *Stress-strain diagram for the First Character of Failure (upper) and the Second Character of Failure (lower)*

In Fig. 40 agreement of both curves in both cases can be seen. This fact validates the proposed experiment in the second part of the thesis and offers future possibilities to analyze the problem more precisely and modify the conditions, setup, loading or boundary conditions of the experiment.

4 CONCLUSIONS

A simple method for objective measuring of the bond in the reference specimens has been found, the configuration of the test and individual parts have been optimized. Now it can be compared to cases with various conditions, e.g. different aggregates or ambient conditions.

The specimens for testing were concrete cylinders with a smooth steel rebar, which was pushed through the specimens. The wanted character of the failure was a shear-only character. Force and bond stress were measured.

Three series of tests were investigated, from each a graph of force-displacement dependence was obtained. The first series resulted in a one-point bending test. The second series followed the intended shear-only test and a linear dependence of applied force and displacement of the rebar could be observed. It also showed a relatively constant bond stress-displacement dependence. The third series showed a second possible character of failure. In future, more tests should be performed to find out which is the dominant character of failure.

If similar specimens as reference specimens are irradiated by gamma radiation and the same repeatable tests are performed, it can be determined whether the bond is affected positively or negatively, the latter being an assumption, or it remains the same.

The results of these and future experiments on irradiated specimens can help greatly in the understanding of gamma and neutron radiation processes and their influence on reinforced concrete. They can be of a global importance in the case of determining the irradiation damage to the NPPs during their service life. These structures cannot be tested or be experimented on as easily as other kinds, therefore, a correlation needs to be found between irradiation and bond.

As the third part of the thesis, a FEM model has been programmed in MATLAB. The numerical model describes the performed experiments and can be used to investigate the alterations of certain aspects of the experiment such as loading, boundary conditions, setup or environmental conditions. Due to the model, the behavior of the model could be determined and validated future experiments. A nonlinear analysis was performed using the iterative Modified Newton-Raphson method. The nonlinear analysis was displacement-controlled to comply with the performed experiments. The force-

displacement curves were fitted to the equivalent charts obtained from the experiments in the second part of the thesis by adjusting the input stress-strain diagrams with specified strengths of the bond elements – the only elements analyzed nonlinearly.

The ability to fit the FEM model to the experiment provides an important tool for the future work when the tests on irradiated specimens may be performed. The FEM model can be adjusted and compared to the results, which can be validated with the experimental data.

The developed method, which is designed primarily for assessment of radiation-induced degradation of the steel-concrete bond, can be readily used for investigation of the effect of various concrete constituents and steel grades and other influential factors on the steel-concrete bonding performance which ultimately decides serviceability of nuclear facilities.

BIBLIOGRAPHY

- [1] The World Nuclear Industry Status Report *Worldnuclearreport.org*. [online]. 2015 [cit. 2018-10-05]. Reachable from: <https://www.worldnuclearreport.org/The-World-Nuclear-Industry-Status-Report-2017-HTML.html>
- [2] Nuclear Forensic Search Project. *Metadata.berkeley.edu* [online]. [cit. 2018-09-20]. Reachable from: <http://metadata.berkeley.edu/nuclear-forensics/Decay%20Chains.html>
- [3] Ochrana při práci se zdroji ionizujícího záření. Dům techniky Ostrava, 1998. ISBN 80-02-01230-5.
- [4] Chemistry: The Central Science, Chapter 21, Section 9. *Wps.prenhall.com* [online]. [cit. 2018-09-20]. Reachable from: <http://wps.prenhall.com/wps/media/objects/3313/3392670/blb2109.html>
- [5] Types of Radiation: Gamma, Alpha, Neutron, Beta & X-Ray Radiation Basics. *Mirion.com* [online]. [cit. 2018-08-31]. Reachable from: <https://www.mirion.com/introduction-to-radiation-safety/types-of-ionizing-radiation/#>
- [6] *Reducing Exposure* [online]. Bakersfield college. [cit. 2018-08-20]. Reachable from: <http://www2.bakersfieldcollege.edu/erp/Radiation/chp6.htm>
- [7] U.S. NAVAL CIVIL ENGINEERING LABORATORY. *Literature Survey of Concretes for Nuclear Radiation Shielding*. 1960, 28 pages. Port Hueneme.
- [8] Iran to Abolish Controls on Iron Ore Pricing | Financial Tribune. *Financialtribune.com* [online]. [cit. 2018-09-20]. Reachable from: <https://financialtribune.com/articles/economy-domestic-economy/61198/iran-to-abolish-controls-on-iron-ore-pricing>
- [9] High Density Concrete | The Construction Civil. *Theconstructioncivil.com* [online]. [cit. 2018-10-02]. Reachable from: <https://www.theconstructioncivil.org/high-density-concrete/>
- [10] Štěpná jaderná reakce. Artemis.osu.cz. [online]. © 2017 [cit. 2017-10-23]. Reachable from: http://artemis.osu.cz/mmfyz/jm/jm_2_3_3.htm

[11] MAKHIJANI, Arjun and Scott SALESKA. *The Nuclear Power Deception: US nuclear mythology from electricity "too cheap to meter" to "inherently safe" reactors*. Apparent First Edition. Rowman & Littlefield Publishers, 1999. 266 pages. ISBN 978-0945257929.

[12] LAMARSCH, John. *Introduction to Nuclear Engineering*. 3rd edition. Pearson, 2001), 783 pages. ISBN 978-0201824988.

[13] Nuclear Power Today | Nuclear Energy – World Nuclear Association. *World-nuclear.org* [online]. [cit. 2018-10-02]. Reachable from: <http://www.world-nuclear.org/information-library/current-and-future-generation/nuclear-power-in-the-world-today.aspx>

[14] PAPE, Yann Le. Structural effects of radiation-induced volumetric expansion on unreinforced concrete biological shields. In: *Nuclear Engineering and Design* [online]. Volume 295, December 15th, 2015. [cit. 2018-10-02]. Reachable from: <https://www.sciencedirect.com/science/article/pii/S0029549315004215>

[15] ŠTEMBERK, Petr. Když se podívám na jadernou elektrárnu, vidím beton. *Technicall*. 3/2015, 32-33. ISSN 1805-1030.

[16] Containment Building – Nuclear Power. *Nuclear-power.net* [online]. [cit. 2018-10-04]. Reachable from: <https://www.nuclear-power.net/nuclear-power-plant/containment-building/>

[17] 2012-2013 Information Digest, U.S. Nuclear Regulatory Commission, NUREG-1350, Vol. 24 , August 2012.

[18] Stainless Steel Reinforcing Bar (Rebar). In: *Stainless-uk.co* [online]. [cit. 2018-10-11]. Reachable from: https://www.stainless-uk.co.uk/site/assets/files/1517/re_bar_0003.png

[19] EN 1992-1-1. Eurocode 2: Design of concrete structures – Part 1-1: General rules and rules for buildings. European Committee for Standardization, 2004.

[20] HOHMANN Brian P., Thomas C. ESSELMAN and James J. WALL: Irradiated Concrete in Nuclear Power Plants: Bridging the Gap in Operational Experience. In: *Inis.iaea.org* [online]. International Atomic Energy Agency, 2012. [cit. 2018-10-02]. Reachable from: https://inis.iaea.org/collection/NCLCollectionStore/_Public/43/070/43070885.pdf

[21] HILSDORF H.K., KROPP J. and H.J. KOCH. The Effects of Nuclear Radiation on the Mechanicals Properties of Concrete. American Concrete Institute Special Publication SP55 1978, pp. 223-251.

[22] Michal OLSZACKI et al. Measurement of the High Gamma Radiation Dose Using the MEMS Based Dosimeter and Radiolysis Effect. In: MicroMechanics Europe Workshop, September 2013, Espoo, Finland. pp. 31-35.

[23] Kontani, O. et al. Irradiation Effects on Concrete Durability of Nuclear Power Plants. Proceedings of ICAPP 2011 Conference (Paper 11361). Nice, France, May 2-5, 2011.

[24] ACI Standard 349.3R-02: Evaluation of Existing Nuclear Safety-Related Concrete Structures. American Concrete Institute. Farmington Hills, MI. 2002.

[25] Naus, D.J. and H.L. Graves III. Primer on Durability of Nuclear Power Plant Reinforced Concrete Structures-A Review of Pertinent Factors. US Nuclear Regulatory Commission. Report No. NUREG/CR-6927 (ORNL/TM-2006/529). pp.112. Feb. 2007.

[26] Assessment and Management of Ageing of Major Nuclear Power Plant Components Important to Safety: Concrete Containment Buildings. IAEA-TECDOC-1025. International Atomic Energy Agency. pp. 162. 1998.

[27] HONG Sungnam and Sun-Kyu PARK. Uniaxial Bond Stress-Slip Relationship of Reinforcing Bars in Concrete. In: *Advances in Materials Science and Engineering* [online]. April 2012. [cit. 2018-10-11]. Reachable from: https://www.researchgate.net/publication/258383542_Uniaxial_Bond_Stress-Slip_Relationship_of_Reinforcing_Bars_in_Concrete

[28] Joint Institute for Power and Nuclear Research – Sosny | Gamma installation UGU420. *Sosny.bas-net.by* [online]. [cit. 2018-10-11]. Reachable from: <http://sosny.bas-net.by/technologies/ugu>

[29] *Chapter 9 – Axisymmetric Elements* [online]. The University of Memphis. [cit. 2018-12-08]. Reachable from: http://www.ce.memphis.edu/7117/notes/presentations/chapter_09.pdf?fbclid=IwAR30EZMLeUiRHE2qMJUysBKVdyp4M72IGy8EEeOqqQROZ55e2YxpABEtLuk

[30] *Lecture 4 – Plane Stress/Strain and Singularities* [online]. Phoenix Analysis & Design Technologies (PADT). [cit. 2018-12-08]. Reachable from: http://www.padtinc.com/mae323/lecture4_plane_stress_and_singularities.pdf

[31] MASHAYEKHI, Mohammad. Multi-Point Constraints- Lagrange Multiplier Method. In: *Mashayekhi.iut.ac.ir* [online]. Isfahan University of Technology, 2017. [cit. 2018-12-09]. Reachable from: https://mashayekhi.iut.ac.ir/sites/mashayekhi.iut.ac.ir/files//files_course/lesson_16.pdf

[32] *2011 Solidworks HELP – Nonlinear Static Analysis* [online]. Dassault Systèmes SolidWorks Corp., ©2014. [cit. 2018-12-10]. Reachable from: <http://help.solidworks.com/2011/english/SolidWorks/sldworks/LegacyHelp/Sldworks/Overview/StartPage.htm>

[33] KIM, Nam-Ho. *Introduction to Nonlinear Finite Element Analysis* [online]. US: Springer, 2015. [cit. 2018-12-10]. ISBN 978-1-4419-1746-1.

LIST OF FIGURES

- Fig. 1** Age Distribution of Operating Reactors in the World as of June 2017
- Fig. 2** The Actinium Series
- Fig. 3** The Penetration Force of Alpha, Beta and Gamma Radiation in the Human Body
- Fig. 4** Diagram of Different Kinds of Radiation and Shielding Options
- Fig. 5** Example of Iron Ore
- Fig. 6** Nuclear Electricity Production Worldwide, April 2018
- Fig. 7** Location of BSC in a Nuclear Reactor
- Fig. 8** License Renewals Granted for Operating Nuclear Power Reactors in USA as of 2013
- Fig. 9** Ribbed Reinforcement Bars
- Fig. 10** Compressive Strength of Concrete Exposed to Neutron Radiation f_{eu} Related to Strength of Untreated Concrete f_{cuo}
- Fig. 11** Volume Change of Aggregates and Hardened Cement Paste During Radiation with Fast Neutrons
- Fig. 12** Compressive and Tensile Strength of Concrete Exposed to Gamma Radiation f_{eu} , Related to Strength of Untreated Concrete f_{cuo}
- Fig. 13** Bond Stress-slip Relationship
- Fig. 14** Typical Stress Distributions for (a) One Side Pull-out, (b) Both Sides Pull-out, and (c) Axial Tension
- Fig. 15** Universal Gamma Installation UGU – 420
- Fig. 16** Dimensions of the Specimen
- Fig. 17** Scheme of the Test
- Fig. 18** Additional Reinforcement in the First Series of Tests
- Fig. 19** Assumed Reduction of Internal Forces, First Series of Tests
- Fig. 20** Damage to the Specimen in the First Series of Tests

- Fig. 21** Dependence of Applied Force and Displacement in the First Series of Tests
- Fig. 22** The Intact Specimen in the Second Series of Tests
- Fig. 23** Dependence of Applied Force and Displacement in the Second Series of Tests
- Fig. 24** The Imperfections Present in Specimen 2 in the Second Series of Tests
- Fig. 25** Dependence of Bond Stress and Displacement in the Second Series of Tests
- Fig. 26** Specimens of the Third Series of Tests – S-Serpentine Aggregate, K-Quartz Aggregate
- Fig. 27** Dependence of Applied Force and Displacement in the Third Series of Tests
- Fig. 28** Dependence of Bond Stress and Displacement in the Third Series of Tests
- Fig. 29** Axisymmetric Problem of a Circular Structure Reduced to a Section and the Corresponding Finite Element Mesh
- Fig. 30** Triangular Torus with Principal Axes r and z and the Circumferential θ Coordinate
- Fig. 31** Triangular Mesh of the Problem with Supports and Loading
- Fig. 32** Triangular Mesh of the Problem with Multi-point Constraints in the Bond Layer
- Fig. 33** Scheme of the Lagrange Multiplier Method
- Fig. 34** Example of the Incremental Displacement Control Method
- Fig. 35** Incremental Control Techniques – Load Control (on the left), Displacement Control (in the middle) and Arc-Length Control (on the right)
- Fig. 36** Iterative Solution Methods – Diagram of One Step in the NR Method Scheme
- Fig. 37** Iterative Solution Methods – Diagram of One Step in the MNR Method Scheme
- Fig. 38** Total Displacements in Directions of Axes r and z
- Fig. 39** Dependences of Applied Force and Displacement from MATLAB Corresponding to the First Character of Failure (upper) and the Second Character of Failure (lower)
- Fig. 40** Comparison of Dependences of Applied Force and Displacement from MATLAB and the Experiment Fitted to the First Character of Failure (upper) and the Second Character of Failure (lower)

Fig. 41 Stress-strain diagram for the First Character of Failure (upper) and the Second Character of Failure (lower)

LIST OF TABLES

Tab. 1 Properties of Heavy Aggregates

Tab. 2 Types of Nuclear Reactors

Tab. 3 Prescription of Concrete in Series 1

Tab. 4 Properties and Origin of Used Aggregates

Tab. 5 Properties of Heavy Aggregates

Tab. 6 Prescription of Concrete in Series 2 and 3

Tab. 7 Results of Series 1, 2 and 3 – Maximum Applied Forces and Maximum Bond Stresses